University of Salerno

Department of Physics named after "E. R. Caianiello"

and Department of Mathematics

in agreement with

University of Campania "Luigi Vanvitelli"

Department of Mathematics and Physics

PhD Program:

Mathematics, Physics and Applications

XXIX Cycle - 2017

Curriculum Fisica

Ph.D. Thesis:

Accurate measurements of spectroscopic line parameters of atmospheric
relevant molecules

Candidate

Tatiana A. Odintcova

Tutor   Coordinator

Prof. Livio Gianfrani   Prof. Sandro Pace

ACKNOWLEDGEMENTS

Content

1. Introduction

Spectroscopy involves the interaction of electromagnetic radiation with matter. Electromagnetic radiation from microwave range to X-rays interacts with matter. Absorption spectra in different spectral ranges arise from the excitation of certain intramolecular motions. Microwave spectra correspond to molecular end-over-end rotations. Absorption spectra of infrared and visible region arise from vibration motion of the atoms. Absorption of X-rays and UV radiation is caused by transitions of electrons in atoms and molecules.

Laser spectroscopy is a reliable and powerful tool to get knowledge about matter. In particular, absorption spectra allows one to characterize the molecular structure and interaction with surrounding molecules. Specifically, measurements of the center frequency of absorption lines enable for the determination of the energy levels, lengths and angles of intramolecular bonds. From the line intensity measurements spatial charge distribution and transition probability can be obtained. From pressure broadening and shifting parameters of spectral lines, information about collision processes and intermolecular potentials can be extracted. The Doppler linewidth can be attributed to the velocity distribution of the molecules, and, consequently, to the temperature of the gaseous sample.

Besides fundamental science, accurate measurement of spectroscopic parameters is necessary for many inverse spectroscopic problems, including in particular global monitoring of atmosphere, requiring determination of concentration of major and minor constituents, such as H_2O, CO_2, O_3, CH_4, N_2O, C_2H_2. In spite of small concentration, these

molecules take part in physical and chemical atmospheric processes and influence on global radiation balance.

For a proper accounting of radiation absorption and propagation in the atmosphere spectroscopic databases were created. The databases include spectroscopic parameters of atmospheric molecules, that are necessary for their spectra modeling, and for accounting radiation propagating in the atmosphere. The best known are HITRAN [1,2] and GEISA [3,4]. Every update of these databases include new and more accurate parameters of more and more transitions of larger number of molecules. High accuracy of the spectroscopic data is crucial for remote sensing because atmospheric absorption calculations assume very long traces with varying conditions, such as pressure, temperature and concentration. Thus, even small uncertainty of spectroscopic parameters leads to significant uncertainty of obtained results. Accurate experimental measurement of line intensities is much harder, than of other spectroscopic parameters. Typical uncertainties for experimental line intensity data are 3% to 10% [5-7], and even high quality measurements (e.g. [8]) usually provide uncertainties in the 1% to 3% range.

This thesis deals with high accuracy measurements of line shape parameters of molecules of atmospheric interest, such as acetylene C_2H_2 and carbon dioxide CO_2 including line intensity factors, pressure broadening and shifting coefficients.

Carbon dioxide CO_2 is one of principal absorbing gases of the Earth atmosphere. Possibility to absorb radiation in the IR domain leads to significant influence of CO_2 concentration on greenhouse effect, and thus, on radiation budget of the Earth atmosphere with consequential climate change. Because of human industrial activities worldwide emission of CO_2

increased significantly during last decades. Carbon dioxide is also prevalent in the atmospheres of some Solar system planets, such as Venus and Mars [9]. Having several absorption bands of different intensity, carbon dioxide is a good marker for probing atmospheres to different depths [10].

There are numbers of missions aimed at measurements of global concentration of CO_2, as well as spatial distribution of CO_2, how sources and sinks of the carbon dioxide vary with seasons, years and locations. For instance, OCO-2 (NASA Orbiting Carbon Observatory) [11,12], GOSAT (Greenhouse Gases Observing Satellite) [10,13] and CarbonSat (preparing to launch) [14], aimed at measurements of CO_2 concentration at 1 ppm level. Absorption bands near 1.6 and 2 µm are used for CO_2 concentration measurements. Thus, uncertainty of spectroscopic parameters (specifically of line intensity) corresponding to transitions of these bands better than 0.5% is necessary, instead of it the HITRAN database provides line intensities in these bands with a relative uncertainty between 2 and 5 %. Since the last edition of the HITRAN database, there have been a large number of experimental [15, 16] and theoretical [16, 17] investigations of carbon dioxide spectra, mainly aimed at support of OCO-2 mission [11,12]. Recent *ab initio* calculations [16, 17] for all atmospherically important CO_2 bands declares accuracy of line intensity better than 0.5 %. Before using results of these calculations they should be tested against the experimental measurements at least for a number of lines. The results of such test will be presented in this work.

Acetylene C_2H_2 is another minor constituent of Earth atmosphere [18,19]. Also, it has been detected in many astrophysical objects: planets, including Mars [20], Jupiter [21], Titan [22], Uranus [23, 24], and Neptune

[25], comets [26], accretion disks of young stars [27], interstellar medium [28], carbon stars [29].

Production of C_2H_2 in the Earth's atmosphere results from human activities related to combustion of hydrocarbon, from fossil, bio fuels and biomass burning, and chemical industries. Its destruction occurs by reaction with OH radicals, ozone, and other oxidants. As a result, its influence on the Earth's climate is quite significant and accurate reconstructions of vertical profiles of this trace gas are of particular relevance. Being long-life atmospheric species and having intense spectroscopic features in IR atmospheric windows C_2H_2 can be remotely observed. This allows to use C_2H_2 as an indicator of combustion sources and as a tracer for atmospheric transport processes and chemistry [30].

C_2H_2 is a linear and light molecule, thus presenting spectra with regular rotational structure with strong isolated and well tabulated lines in the IR. C_2H_2 is stable gaseous species, thus easily handled. It is linked to experimental advances in high-resolution molecular spectroscopy, as species to test. It was used to test or elaborate a variety of instrumental approach. Because of these benefits acetylene is being used as a molecular target for the spectroscopic determination of the Boltzmann constant by means of Doppler Broadening Thermometry (DBT) (see [31] and reference therein). The latter task is one of prime challenges of modern molecular spectroscopy. Fulfillment of the task requires considerable improvement of the target line shape parameters entailing achievement of an extraordinary level of experimental abilities.

In a view of aforesaid the aims of this work are:

1) Development of the new approach based on OF-CEAS technique and optical frequency comb for high accuracy CO_2 line intensity measurements.

2) Optimization of the dual-laser spectrometer [32] and further increase of measurements accuracy of C_2H_2 line spectroscopic parameters. A further aim of this thesis is the optimization of Doppler-broadening thermometry as a primary method for the spectroscopic determination of the gas temperature, for the aims of the practical realization of the new Kelvin.

Structure of the work

The basic absorption spectroscopy equations used in this work and particular experimental techniques implemented in the design of the considered spectrometers are given in the second chapter.

The third chapter is devoted to development of spectrometer operating at 2 μm and based on Optical Feedback Cavity Enhanced Absorption Spectroscopy (OF-CEAS) technique and optical frequency comb. This approach provides absolute frequency scale underneath recorded absorption spectrum. The spectrometer was used for measurements of CO_2 line shape parameters, specifically line intensities, of transitions of band 20012-00001. Unprecedented accuracy of the measured line intensity was obtained. Obtained values of measured line intensities demonstrate agreement at the subpercent level with recent most accurate to date theoretical calculations [16].

The forth chapter is dedicated to spectroscopic parameters measurements (intensity, pressure broadening and shifting coefficients) of C_2H_2 transition around 1.39 μm. The dual-laser approach based on optical phase-locking was implemented. The dual laser absorption spectrometer is based on a pair of offset frequency locked lasers, one being the reference laser and the other, the probe laser, that acts as a frequency standard based

on noise-immune cavity-enhanced optical heterodyne molecular spectroscopy. This approach provides an absolute frequency scale underneath the absorption spectra. The spectroscopic parameters was measured with subpercent uncertainty. Application of obtained results to DBT was also considered.

In the conclusion main results of the thesis are summarized.

2. Absorption spectroscopy: used methods and techniques

2.1. Beer-Lambert law

Attenuation of the laser power transmitted through the cell filled with absorbing gaseous sample is described by the Lambert-Beer law:

$$\frac{I(v)}{I_0} = e^{-\alpha(v) \cdot L}, \tag{2.1}$$

where v is frequency of the radiation, I_0, $I(v)$ are incident and transmitted power respectively, L - absorption path length, and $\alpha(v)$ is absorption coefficient of matter per unit of length (cm^{-1}), that is function of radiation frequency. Considering isolated resonance line corresponding to transition between ro-vibrational energy levels, the absorption coefficient can be represented as

$$\alpha(v) = S(T)g(v - v_0)N, \tag{2.2}$$

where $S(T)$ is a line strength as function of temperature (*cm/molecule*), v_0 is line center frequency (*cm^{-1}*), $g(v-v_0)$ is normalized line shape function ($\int g(v - v_0) = 1$) and N is a number density of the absorbers (*molecules/cm^3*). Therefore, Lambert-Beer law can be presented in a following way:

$$\frac{I(v)}{I_0} = e^{-S(T)g(v - v_0)NL}. \tag{2.3}$$

The integrated absorbance A is defined as an area under the observed spectrum over a whole spectral profile, as follows:

$$A = -\int \ln\left(\frac{I(v)}{I_0}\right) dv = \int S(T)g(v - v_0)NLdv = S(T)NL. \tag{2.4}$$

As it follows from (2.2) and (2.4), absorbance $\alpha(v) \cdot L$ is defined as

$$\alpha(v) \cdot L = A \cdot g(v - v_0). \tag{2.5}$$

13

2.2. Line shape parameters

The line shape profile of an isolated transition is defined by three major physical factors: natural broadening, Doppler broadening and collisional broadening. Accurate evaluation of the line shape profile requires taking into consideration the "wind" effect (the speed dependence of collisional cross-section) and Dickie narrowing (the averaging effect of velocity changing collisions).

The natural broadening of a spectral line is due to the Heisenberg uncertainty principle. Molecules can absorb radiation within a frequency range (namely, the line width), which is determined by molecular lifetime related to spontaneous transitions between a given pair of energy levels. Natural broadening results in Lorentzian line shape profile, but for ro-vibrational transitions of most atmospheric molecules at typical for atmosphere conditions influence of this mechanism is negligible in comparison with others.

The frequency of the electromagnetic radiation propagating along the y-axis, that is experienced by moving molecules, differs from the static one v_0 by the term of $\Delta v = \pm \left(\dfrac{V_y}{c} \right) v_0$, where V_y - speed f molecule along y-axis, and c - speed of light. Considering the Maxwell distribution of the speed of molecules at the thermodynamic equilibrium, one can obtain the Doppler-broadened profile, which is given by a Gaussian function:

$$f_D = \sqrt{\frac{2 \ln 2}{\pi}} \frac{1}{\Gamma_D} \exp \left(-\ln 2 \left(\frac{v - v_0}{\Gamma_D} \right)^2 \right) , \qquad (2.6)$$

where $\Gamma_D = \dfrac{v_0}{c} \sqrt{\dfrac{2 k_B T}{M} \ln 2}$ is Doppler width (half-width at half maximum, HWHM) and k_B is the Boltzmann constant.

14

Collisions between molecules lead to changes of the quantum state of both absorbing and perturbing molecules, which leads to a reduction of the life time of the initial and final states of the transition and results in additional line broadening, called collisional broadening. Collisions may also produce pressure-dependent shifting of the transition frequency. General influence of collisions to the line shape is described by Lorentz function:

$$f_L(v - v_0) = \frac{1}{\pi} \frac{\Gamma}{(v - v_0 - \Delta)^2 + \Gamma^2} , \qquad (2.7)$$

where Γ - pressure broadened line width and Δ is pressure-induced line shift.

Doppler effect prevails at low pressures, while the effect of collisions dominates at high pressures. For intermediate pressures both effects are important. Line shape that takes into account both, Doppler and collisional broadening, is a convolution of these two profiles:

$$f_V(v, v_0) = \int f_D(t, v_0) \cdot f_L(v - t, v_0) dt . \qquad (2.8)$$

This is so-called Voigt profile incorporating three parameters: Doppler width Γ_D, collisional width Γ and shift Δ.

With improving of signal-to-noise ratio of experimental spectra up to about 1000 it becomes evident, that Voigt profile does not fit real line shape and that consideration of other fine effects is necessary. The observed lines are higher and narrower, than it follows from the Voigt profile. The deviations from the Voigt profile are attributed to the effect of collisional velocity changes (preserving the coherence with the field), which efficiently reduce Doppler width Γ_D, and speed dependence of the relaxation rates, which correct the collisional profile for different velocity-classes of active molecules.

The effect of collision-induced velocity changes is usually known as Dicke narrowing [33]. The presence of the intermolecular collisions, which do not affect the internal state of the active molecule, and leads to velocity changes, results in reduction of the Doppler line width. The effect is usually described by the soft collision model (Galatry profile) [34] or by the hard collisions model (Rautian profile) [35].

The Galatry absorption profile was derived in the framework of the Brownian motion model [36]. The model supposes that number of collisions is necessary to change velocity of the molecule significantly. Within the Rautian model, the profile was constructed by using the method of the kinetic Boltzmann equation. The model assumes that molecular velocities before and after each collision are completely decorrelated, i.e. molecule loses completely the memory of its previous velocity and a new velocity follows Maxwell distribution.

Both models introduce one extra lineshape parameter β, optical diffusion rate, to quantify the frequency of velocity changing collisions. Previous studies [37,38] have shown that β should be smaller than the kinetic diffusion rate

$$\beta_{kin} = \frac{kT}{MD},\tag{2.9}$$

where M - molecular mass, D - diffusion coefficient.

The wind effect is the dependence of the collisional relaxation rate on the absolute speed of the absorbing molecule [39]. Speed dependences of the relaxation rates leads to Speed Dependent Voigt Profile. The simplest and the most common way to introduce speed dependence is quadratic approximation [40]:

$$\Gamma(V_a) = \Gamma_0 \left\{ 1 + \gamma_2 \left(\left(\frac{V_a}{V_{a0}} \right)^2 - \frac{3}{2} \right) \right\},\tag{2.10}$$

$$\Delta(V_a) = \Delta_0 \left\{ 1 + \delta_2 \left(\left(\frac{V_a}{V_{a0}} \right)^2 - \frac{3}{2} \right) \right\}, \quad (2.11)$$

where Γ_0 and Δ_0 characterize the dependence on the active molecular velocity V_a (V_{a0} is the most probable value).

Both speed dependence and Dickie effects take place simultaneously. Speed Dependent Rautian Profile (SDRP) and Speed Dependent Galatry Profile (SDGP) take into account both effect. These models assume that velocity changing and rotation state changing aspects of collision are independent. But change of velocities is balanced by a change of the colliders internal states. Therefore, both velocity changing and speed dependent mechanisms operate simultaneously and their parameters are correlated.

To take into account all these effects on line shape profile the *HTP* profile (Hartmann-Tran Profile or partially Correlated quadratic-Speed-Dependent Hard-Collision Profile) can be used [41].

In comparison with other, more sophisticated line shape profiles (for example, SDDRGP [42]), accounting for the Dicke narrowing effect, the speed dependence of line broadening, and the partial correlation between velocity- and phase-changing collisions, the *HTP* can be presented in a relatively simple form and thus, rapidly computed. That is why it was recommended by IUPAC (International Union of Pure and Applied Chemistry) for using instead of the Voigt profile when high line shape description accuracy is required [43].

HTP includes 7 parameters: the Doppler width Γ_D, the mean collisional relaxation rate Γ_0, the mean collisional shift of the line center Δ_0, the parameter accounting for the speed dependence of the collisional broadening γ_2 and shifting δ_2, the frequency of velocity changing collisions

$\boldsymbol{\beta}$ and the parameter representing the partial correlation between velocity and rotational state changes due to collisions $\boldsymbol{\eta}$. Thus, the HTP profile can be expressed as follows:

$$HTP(v) = \frac{1}{\pi} \text{Re} \left\{ \frac{A(v)}{1 - \left[v_{VC} - \eta \left(C_0 - \frac{3C_2}{2} \right) \right] A(v) + \left(\frac{\eta C_2}{v_{a0}^2} \right) B(v)} \right\}, \qquad (2.12)$$

where *A(v)* and *B(v)* are represented by the complex probability function *w(z)*

$$A(v) = \frac{\sqrt{\pi} c}{v_0 v_{a0}} [w(iZ_-) + w(iZ_+)], \qquad (2.13)$$

$$B(v) = \frac{v_{a0}^2}{\widetilde{C}_2} \left[-1 + \frac{\sqrt{\pi}}{2\sqrt{Y}} (1 - Z_-^2) w(iZ_-) - \frac{\sqrt{\pi}}{2\sqrt{Y}} (1 - Z_+^2) w(iZ_+) \right], \qquad (2.14)$$

$$w(z) = \frac{i}{\pi} \int_{-\infty}^{+\infty} \frac{e^{-t^2}}{z - t} dt = e^{-z^2} erfc(-iz). \qquad (2.15)$$

In these expressions $Z_\pm$, *X, Y,* are given by the equations:

$$Z_\pm = \sqrt{X + Y} \pm \sqrt{Y},$$

$$X = \frac{i(v_0 - v) + \widetilde{C}_0}{\widetilde{C}_2}, \qquad (2.16)$$

$$Y = \left(\frac{v_0 v_{a0}}{2c\widetilde{C}_2} \right)^2.$$

where *c* is speed of light in vacuum and C_0 , C_2 and v_{a0} are defined by

$$\widetilde{C}_0 = (1 - \eta) \left(C_0 - \frac{3C_2}{2} \right) + v_{VC},$$

$$\widetilde{C}_2 = (1 - \eta) C_2,$$

$$C_0 = \Gamma_0 + i\Delta_0, \qquad (2.17)$$

$$C_2 = \gamma_2 \Gamma_0 + i(\delta_2 \Delta_0),$$

$$v_{a0} = \sqrt{\frac{2k_B T}{M}},$$

where v_{a0} is the most probable speed of molecules with mass M at temperature T, k_B is Boltzmann constant. The dependence of the relaxation rate on molecular speed v_a is defined by the quadratic function (2.10) as was suggested in [39].

The *HTP* profile was used for analysis of the data obtained in the current work.

2.3. High finesse cavities

Cavity resonance can be used in absorption spectroscopy for the considerable enhancement of electromagnetic field within narrow spectral interval. High finesse optical cavities attract an interest in the field of high-sensitivity gas phase spectroscopy.

Fabry Perot resonators are composed of two spherical (or flat) mirrors with radiuses of curvature R_1 and R_2 parallel to each-other, facing each other and separated by the distance L. Standing optical wave can be formed between the mirrors. Depending on the relation between R_1, R_2 and L, al resonators can be divided in following configurations: plane-parallel cavity ($R_1=R_2=\infty$); spherical cavity ($R_1=R_2=L/2$); hemispherical cavity ($R_1=\infty$, $R_2=L$); confocal cavity ($R_1=R_2=L$); convex-concave cavity (R_1-$R_2=L$).

If arbitrary beam successively reflected from both mirrors moves away from the cavity axis, the resonator is not stable. But if the beam is kept inside limited area, the resonator is stable.

Stability of laser resonators is defined by the relation of radius of curvature of two mirrors and their separation, fulfillment of the conditions is necessary to provide stable localization of light inside the cavity:

$$0 < \left(1 - \frac{L}{R_1}\right)\left(1 - \frac{L}{R_2}\right) < 1. \tag{2.18}$$

Laser beams are similar to plane waves, but their intensity distributions are not uniform, they are concentrated near the axis of propagation and their phase fronts are slightly curved. Intensity distribution of laser beam is Gaussian in every cross section, width of Gaussian intensity profile changes along the axis. Considering that the Gaussian beam has its minimum diameter $2w_0$ at the beam waist, where the phase

front is plane, radius of the beam or "spot size" *w(z)* (the transverse distance at which the amplitude of electrical field is 1/e times that on the axis) in the plane that intersects the propagation axis at *z* is

$$w^2(z) = w_0^2 \left[1 + \left(\frac{\lambda z}{\pi \omega_0^2} \right)^2 \right],$$
(2.19)

and radius of curvature *R(z)* of wave-front that intersects the axis at z is

$$R(z) = z \left[1 + \left(\frac{\pi \omega_0^2}{\lambda z} \right)^2 \right].$$
(2.20)

Resonator with two plane mirrors does not support Gaussian beam. It can be coupled into spherical or hemispherical cavity. A mode of resonator is defined as self-consistent field configuration, and can be represented by a wave beam propagating back and forth between the mirrors, and the beam parameters must be the same after one complete round trip of the beam. As the beam travels in both directions between the mirrors it forms the axial standing wave pattern that is expected for a resonator mode [44]. During each round trip, a portion of light leaks out through the cavity mirrors at a rate proportional to the intracavity losses.
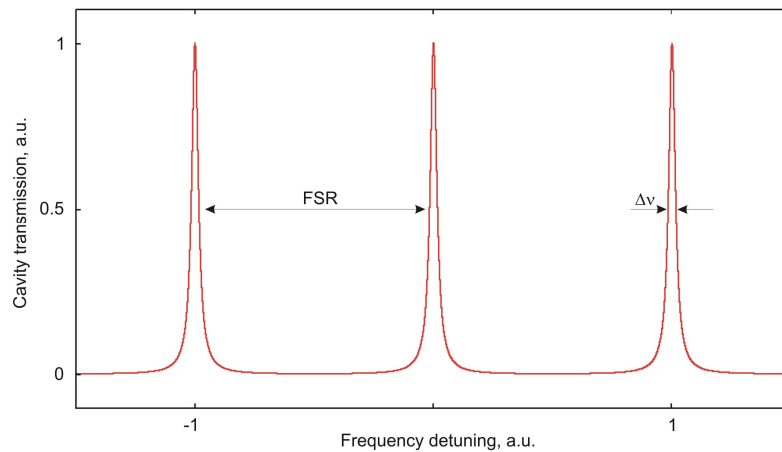

Fig. 2.3.1. Transmission of the cavity

As it is shown in Fig. 2.3.1. transmission of the cavity is represented by comb of resonances (eigen modes of the cavity) equally spaced by free spectral range $FSR = \dfrac{c}{2L}$. Transmitted intensity is given by the well-known Airy formula:

$$I_{out}(\omega) = I_{in} \frac{T^2}{(1-R)^2} \frac{1}{1 + \left(\dfrac{2\sqrt{R}}{1-R}\right)^2 \sin^2\left(\dfrac{\omega t_r}{2}\right)}, \qquad (2.21)$$

$$R = \sqrt{r_1 r_2}, \quad T = \sqrt{t_1 t_2},$$

where t, r - field transmission and reflection coefficient of the two cavity mirrors. Around a resonant frequency the transmitted intensity given by eq. (2.21) is well approximated by a Lorentzian function. Full width at half maximum (FWHM) of this resonance is $\Delta v = \dfrac{1}{\pi t_r} \dfrac{1-R}{\sqrt{R}}$. Width of the resonances and cavity FSR define cavity finesse and Q-factor:

$$F = \frac{FSR}{\Delta v} = \pi \frac{\sqrt{R}}{1-R}, \qquad (2.22)$$

$$Q = \frac{v}{FSR} F, \qquad (2.23)$$

where v - optical frequency of excitation. The higher reflectivity of the mirrors, the narrower the cavity modes, and higher cavity finesse. It is worth to mention, that resonances of high-finesse cavity can be spectrally narrower than the laser. Ring down time τ_{RD} or the photon lifetime in the cavity is defined by the cavity resonance width Δv:

$$\tau_{RD} = \frac{1}{\pi \Delta v} \frac{1-R}{\sqrt{R}} = \frac{L}{c} \frac{\sqrt{R}}{1-R}. \qquad (2.24)$$

2.4. Optical frequency comb

Since the optical frequency comb has been invented [45,46] it found applications in laser spectroscopy as an optical ruler. Knowing frequencies of the comb teeth one can find frequency of the laser by measurements of the beat note between unknown laser frequency and the comb component frequency. An optical frequency comb consists of lines separated with equal distance in frequency domain and it stretches through up to about an octave. The frequency comb can be obtained by stabilization of the femtosecond pulse train generated by a mode-locked laser. The first demonstration of self-referenced frequency comb generation relied on mode-locked Ti: sapphire lasers [47]. More recently, optical frequency comb generators based on fiber lasers (for example erbium-doped fiber lasers) have also been developed [48]. Fiber sources have the potential for a more practical, robust and compact setup, as required for real-world applications. Frequency comb laser sources are commercially available from different producers.

As it is shown in Fig. 2.4.1 typical fiber laser-based frequency comb system consists of a mode-locked laser oscillator, amplification and a spectral broadening part, a detection unit and control electronics, that stabilize frequencies of the comb lines.

Mode-locked lasers emit a periodic train of femtosecond optical pulses. Electric field of the mode-locked laser pulse, circulating in the laser resonator, can be represented as product of pulse envelope function $e(t)$ and continuous wave with carrier frequency ω_c:

$$E(t) = e(t) \cdot e^{i\omega_c t} . \qquad (2.25)$$

23

Pulse electric field over time is shown in upper panel of Fig. 2.4.2. In the figure ϕ_{ceo} - carrier envelope phase - is the shift between the peak of the envelope and the closest peak of carrier wave.
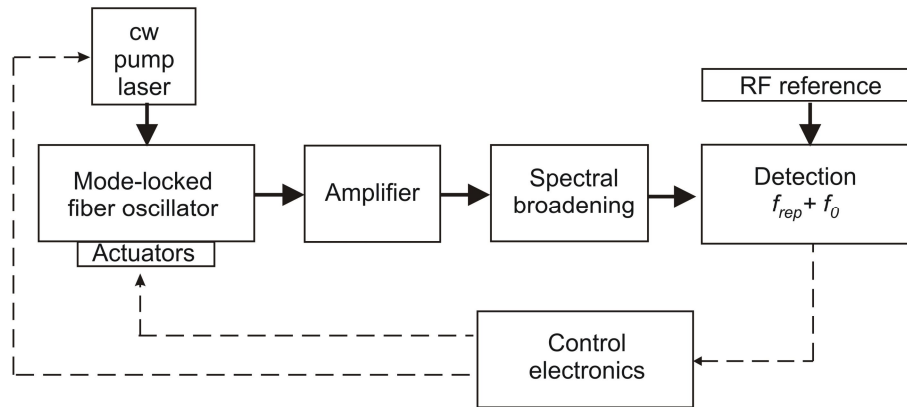

Fig. 2.4.1. Simplified diagram of a typical fiber laser-based frequency comb system. The pulsed output of a fiber laser oscillator is amplified and spectrally broadened. These pulses are then launched into highly nonlinear fiber in which nonlinear processes such as self-phase modulation, self-steepening, four-wave mixing, and Raman scattering spectrally broaden the pulses up to about full octave. The detected signals are used in a control loop for stabilization.

Power spectrum of identical pulses train having any shape and separated by a fixed interval can be obtained by a Fourier series expansion, translating the amplitudes from the time domain to the frequency domain. It results in a comb of regular spaced frequencies, where the comb spacing is defined by the time between pulses, i.e. it is the repetition rate f_{rep} of the laser that is producing the pulses.

Difference between the phase and group velocities inside the cavity for the train of pulses emitted by a mode-locked laser leads to the pulse to pulse change of phase ϕ_{ceo} arises, that is defined as

24

$$\Delta\phi_{ceo} = \left(\frac{1}{\upsilon_g} - \frac{1}{\upsilon_p}\right) l_c \omega_c, \qquad (2.26)$$

where l_c round trip length of the cavity, ω_c is "carrier" frequency.

Considering that ϕ_{ceo} is evolving with time, such that from pulse to pulse there is phase increment of $\Delta\phi_{ceo}$, in the spectral domain shift of line frequencies comes around:

$$f_0 = \frac{1}{2\pi}\frac{\Delta\phi_{ceo}}{T} = \frac{1}{2\pi}f_{rep}\Delta\phi_{ceo}. \qquad (2.27)$$

The optical frequencies f_n of the comb lines are $f_n = nf_{rep} + f_0$, where n is a large integer (of the order of 10^6) that indicates the comb line, f_0 is the offset due to the pulse-to-pulse phase shift, f_{rep} is the repetition rate frequency. The mode-locked laser emits a spectrally narrow and unstable frequency comb. Then, the pulses are amplified and narrowed, so that the spectral broadening section provides the comb covering slightly more than full optical octave. At this point, optical frequency of each comb tooth is not known and not stabilized. The correspondence of time- and freq-domain pictures is presented in Fig. 2.4.2.

The frequency of repetition rate and cavity envelope offset frequency must be stabilized upon frequency standard for absolute frequency measurements. The repetition rate frequency is detected by the fast photodetector (FPD). A servo loop controls the repetition rate of the laser by comparing the FPD signal with a radio frequency (RF) standard. For optical frequency comb generator with the optical spectrum span of an octave in frequency, cavity envelope offset frequency can be obtained applying interferometric measurement. The second harmonic crystal is used to produce doubled in frequency comb lines of the low frequency portion of the spectrum. They will have very close frequencies with the comb lines

on the high frequency side of the spectrum with index *2n*. The beat note between these lines corresponds to the offset frequency $2f_n + f_{2n} = 2(nf_{rep} + f_0) - (2nf_{rep} + f_0) = f_0$. A servo loop controls the offset frequency of the laser by comparing the FPD signal to a frequency standard. f_{rep} and f_0 are controlled by cavity length and pump power respectively.
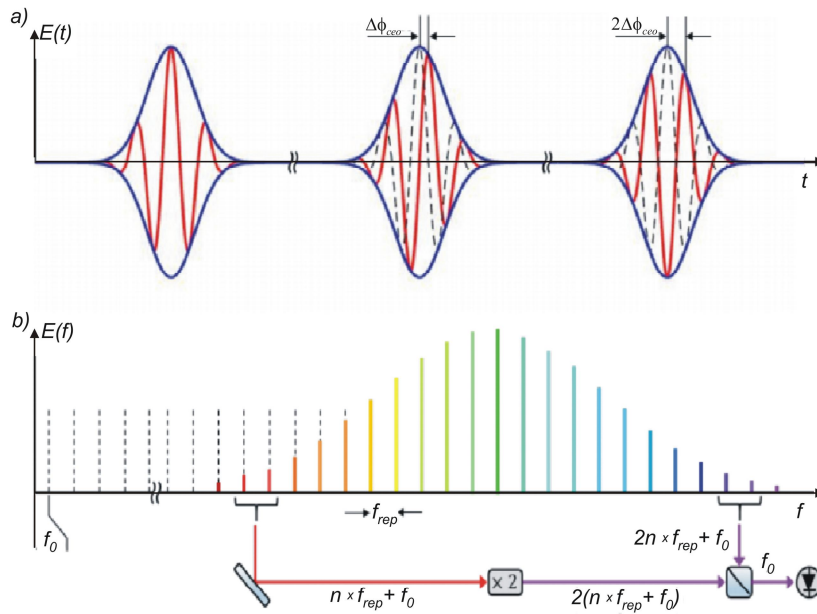
Fig. 2.4.2. Optical pulse train and spectrum emitted by a mode-locked laser. a) The carrier wave (red) and the pulse envelope (blue) travel with different phase and group velocities, leading to a carrier-envelope phase shift. b) The optical spectrum of a mode-locked laser consists of frequency teeth separated by the repetition rate of the laser. The standard method of detecting f_{ceo} with f-$2f$ interferometer is shown.

In the case when f_{rep} and f_0 are stabilized, and thus, all frequencies of the comb teeth are known, any optical frequency within the range of the frequency comb can be determined by recording a beat note between the unknown frequency and the comb tooth. The frequency of the laser f_{DL} can

26

be found as $f_{DL}=f_n\pm f_{beat}$, where f_{beat} is frequency offset (or beat note) between the laser and the nearest in frequency comb line f_n.

2.5. Diode laser frequency locking

High accuracy absorption spectroscopy requires not only absolute and linear frequency scale but also a highly monochromatic source of a probe radiation. Diode laser (DL) has short (µs) coherence time, thus average frequency dispersion (laser spectrum) with FWHM of more than 1 MHz. Growing need of lasers with high spectral purity has stimulated the development of a number of DL frequency stabilization techniques. These techniques are based on: optical feedback (OF) [49], external cavities [50], injection locking [51] and electronic servo control [52]. Because of the spectral characteristics of the diode laser frequency noise, the only systems that are able to achieve substantial linewidth reduction are those that incorporate OF or use very fast electronic servos (with bandwidth more than 20 MHz). In the following two paragraphs these two approaches are described.

2.5.1. Diode laser locking to a cavity

The high sensitivity of the diode lasers to OF is a well-known phenomenon that generally has a disruptive effect on the lasers output frequency and amplitude stability [53]. The sensitivity to OF can be put to advantageous use. The DL coherence may be increased when frequency selected optical field originating from a mode of a high finesse cavity is re-injected into DL. Fabry-Perot cavity can serve as an optical feedback element that forces a diode laser automatically to lock its frequency optically to the cavity resonance. With the appropriate optical geometry the laser optically self locks to the resonance of Fabry-Perot cavity. The

method relies on having optical feedback occur only at the resonance of high finesse cavity.

A feature of the laser locking system [54] represented in Fig. 2.5.1.1 is that there is an optical feedback to the laser only when its frequency matches the resonant frequency of the reference cavity. Confocal cavity in off axis operation is simple and effective configuration for this purpose. The output beam labeled as I is a combination of the reflected from the input mirror beam and resonant field inside the cavity. This beam has a power minimum when the laser frequency matches a cavity resonance. The outputs labeled as II contain only the transmitted cavity resonant field. When the DL frequency does not match to cavity resonance there is no optical feedback and laser frequency scans as usual with changes in the injection current. As the DL frequency approaches a cavity resonance, resonant feedback occur and the DL frequency locks to the cavity resonance, even if the laser current continues to scan [54].
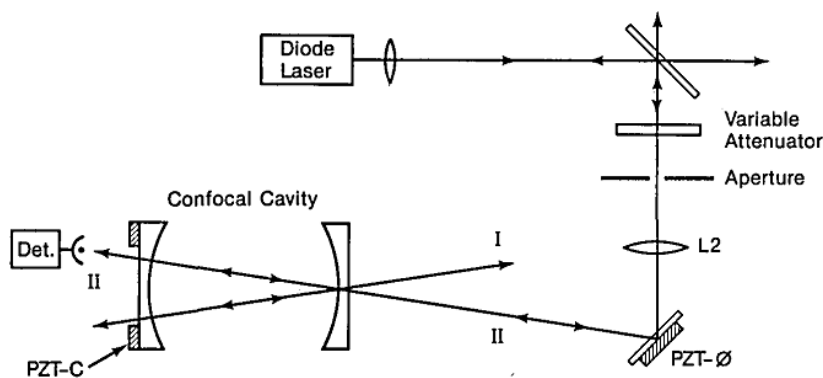

Fig. 2.5.1.1. Schematic the optical feedback locking system [54].

New approach incorporating OF, namely OF-CEAS (Optical Feedback Cavity Enhanced Absorption Spectroscopy) was developed in work [55] for fast and accurate trace gas measurements. Locking to a cavity

with V-geometry with much higher cavity finesse in comparison with confocal cavity was used in [54]. Similar system operating around 2 μm was developed by the authors of the work [56].

The setup consists of a distributed-feedback diode laser (DFB-DL) coupled to the high-finesse ($\sim 10^5$) optical cavity. This latter is mounted in a "V" shape configuration by using three high-reflectivity mirrors (Fig. 2.5.1.2). The idea of the technique is that cavity provides selective optical feedback to the DFB-DL from the intracavity field when the laser frequency coincides with that of one of the cavity modes.

Laser radiation having stable amplitude and large spectral width is injected into the cavity through the folding mirror. Transmitted light possesses a very low spectral width, given by the cavity mode width, but a high level of amplitude fluctuations. When returning part of this radiation into the laser, the saturated gain dynamics dampens those fluctuations. In addition, OF acts as injection seeding at the cavity resonance frequency. Since a DL is a good, low-coherence, broad-band amplifier, injection seeding results in driving the laser field highly monochromatic. Light finally emitted from the laser-cavity loop has stable amplitude with a long coherence time [55]. Such OF with optimized parameters results in substantial reduction of the laser linewidth. For example, for the setup described in [56] in free running conditions the width is about 2 MHz, the action of the OF results in a narrowing of the linewidth to the level of 10 kHz, which is even less than the cavity mode width. This narrow band radiation is frequency locked to one of the cavity mode.

Important parameters for an efficient OF-locking are represented by the feedback rate (that is ratio of the power of light coming back from the cavity to the laser to laser power) and the distance between the laser and

the optical cavity, which determines the phase of the light coming back to the laser [55]. The feedback rate can be regulated by a proper combination of a half-wave plate and a polarizer and constitutes about 10^{-5}. As was shown in [55], optimal laser-to-cavity distance should be about the length of the V-cavity arm. When scanning the laser over successive cavity modes, the wavelength change affects the number of oscillations of the laser field on its way to and from the cavity giving different OF phase. This shifts the locking interval over the resonance profile. The distance can be adjusted in a real time by a mirror mounted on a piezo actuator actively controlled by electronic feedback circuit. Cavity output is monitored by fast 1.5-MHz bandwidth InGaAs photodetector during frequency scan. The feedback circuit employs symmetry of monitored cavity modes to produce an error signal for mirror piezo adjustments.
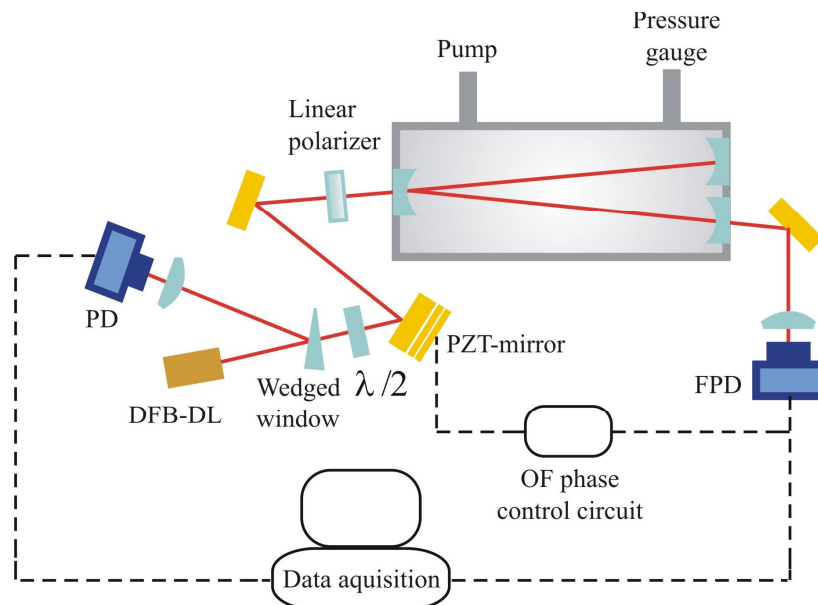
Fig. 2.5.1.2. Sketch of the radiation source of the spectrometer. DFB-DL distributed-feedback diode laser, PD - photodetector, FPD - fast photodetector, λ/2 - half wave plate.
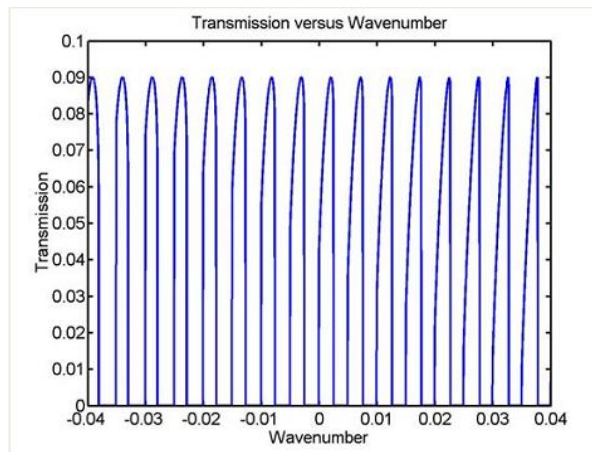
Fig. 2.5.1.3. Transmission signal of the V-cavity.

Locked laser frequency jumps from one resonance to another very quickly passing through the free running condition supplying the stepwise scan. Frequency of the laser is tuned by sweeping its driving current. High quality of radiation on both vertical (intensity) and horizontal (frequency) scales is crucial for high precision measurements. Spectral data points are taken at the frequency comb of the equidistant TEM_{00} cavity modes, which do not move during short time of the laser scan. OF enables injection efficiency orders of magnitude better than without feedback. Thus the setup provides, at the output cavity mirrors, a stable and equally spaced comb-like radiation structure (Fig. 2.5.1.3) in which the frequency distance between two consecutive teeth is determined by the cavity free-spectral range (FSR).

2.5.2. Frequency Locking

Frequency control of the laser can be accomplished by stabilizing its frequency relative to a stable reference (such as another independently stabilized laser), at a precise frequency difference, which is referenced as a frequency locking. Frequency locking allows precise control, stabilization

and synchronization of the probe laser frequency. Frequency locking can be realized by means of optical phase-locking loop (OPLL) or offset frequency locking (OFL).

A first step in both OPLL and OFL requires to detect the beat-note signal between the two lasers using a fast photo-detector. Then (see Fig. 2.5.2.1) the radio frequency beat-note signal is amplified and subsequently scaled in frequency by a factor of N using a divider. Obtained signal is sent to a phase and frequency detector (PSD), which compares it to a reference signal provided by a RF synthesizer thus producing an error signal proportional to the difference of phases between reference and beat-note signals. After, the error signal is properly integrated (providing strong response to slow deviations and moderate response to the fast deviations) and used to continuously lock the frequency of the beat note with frequency of the reference signal. For this purpose, servo system is used. Servo system provides correction signal, that is applied to the laser frequency control electronics. The system allows to actively control the laser emission frequency in such a way that frequency offset between probe laser and reference laser is forced to maintain frequency f_{RF} set by RF synthesizer. The stabilized frequency of the probe laser f_{DL} is defined by RF frequency f_{RF} and frequency of the optical reference f_{ref}: $f_{DL} = f_{ref} \pm N \cdot f_{RF}$. Once the frequency locking loop is activated highly accurate frequency scan of the probe laser frequency can be performed by tuning the RF frequency.

Providing phase coherence between the two lasers, OPLL allows to transfer a long term stability of the reference frequency standard to any frequency of the range under consideration. OPLL represents servosystem, in which phase of the signal under control is adjusted to the phase of high

stable reference signal. A broad bandwidth of the overall control loop electronics is required in this approach to ensure that the optical sources are accurately synchronized, which makes this technique to be very complicated. In many spectroscopic experiments phase coherency is not required and it is sufficient that the probe laser maintains precisely fixed frequency-offset from a reference laser. In this case the control bandwidth can be rather narrow and OFL can be implemented as simpler (one control channel) locking scheme, still ensuring high frequency stability of the radiation.
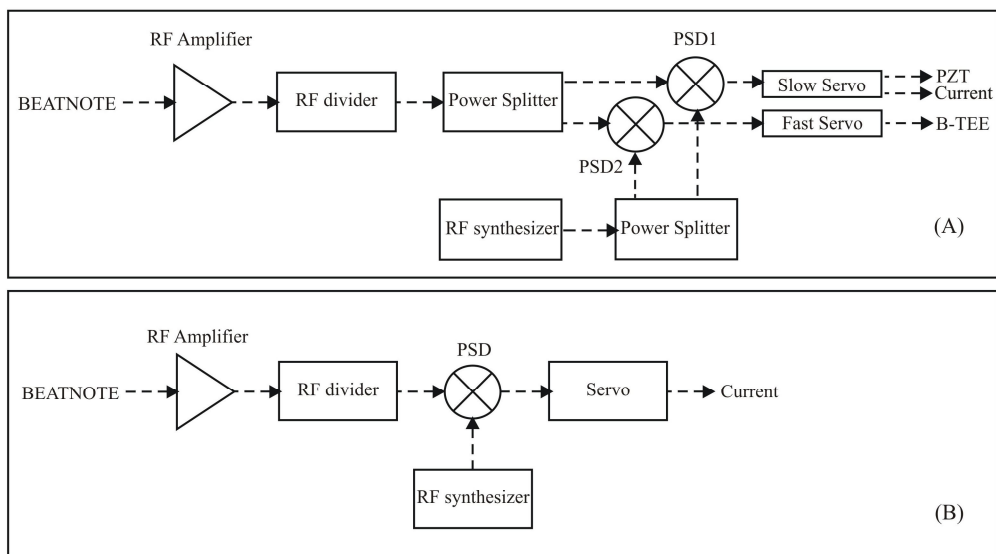
Fig. 2.5.2.1. Scheme of (A) Optical phase-locking loop (OPLL); (B) offset frequency locking (OFL).

Two setups implementing frequency locking were used in the current work. The first scheme was used to control frequency of the external-cavity diode laser (ECDL) working at 1.39 μm. As optical reference an optical frequency standard based on noise-immune cavity-enhanced optical heterodyne molecular spectroscopy (NICE-OHMS) [57] was used. The emission frequency of the second ECDL (serving as a reference laser (RL))

was actively stabilized against the center of a sub-doppler $H_2^{18}O$ line profile, observed under optical saturation conditions in a high-finesse resonator [57]. NICE-OHMS provides a dispersion signal which is employed as an error signal. The emission line width of the RL was carefully determined from measurements of the radiation noise power spectral density at different frequency offsets. The linewidth of the optical frequency standard is about 7 kHz (full width at half maximum) for an observation time of 1 ms [58]. The probe laser (PL) was phase locked to the reference laser by using the broadband phase-locking electronics that is shown in Fig. 2.5.2.1.(A). More specifically, portions of the two laser beams are focused on a fast photodetector (with a bandwidth of 12 GHz) to produce a beat-note signal which is sent to a power amplifier (model RF BAY LPA-8-17), scaled down in frequency by a factor of 40 (by using a frequency divider, model RF BAY FPS-40-12), split into two parts and then sent to a pair of digital phase and frequency detectors. The first one (PSD1, model RF BAY PDF-100) has an integrated loop filter limiting its bandwidth to 10 kHz, while the second (PSD2, model Analog Devices 9901) is much faster. The first PSD ensured a robust and reliable frequency lock in the audio bandwidth (roughly 1 kHz for the loop controlling the extended cavity length and 10 kHz for that acting on the laser current through its driver), whereas PSD2 ensured an effective phase locking between the two lasers directly controlling the diode laser current. A radio-frequency synthesizer (model RHODE&SCHWARZ SMBV100) provides the reference RF signal for both the PSDs, determining the tunable offset frequency between the two lasers. As a result of the action of the third loop, a significant narrowing (down to the Hz level) of the beat-note could be observed (Fig. 2.5.2.2, right). This demonstrates that the PL spectral purity

could be improved up to the limit determined by the RL. The efficient control bandwidth was estimated from the servo bumps that appear in the spectral shape of the closed-loop beat-note signal (Fig. 2.5.2.2, left). Once the laser is locked, its frequency tuning was implemented by changing the frequency offset that is defined by the RF synthesizer.
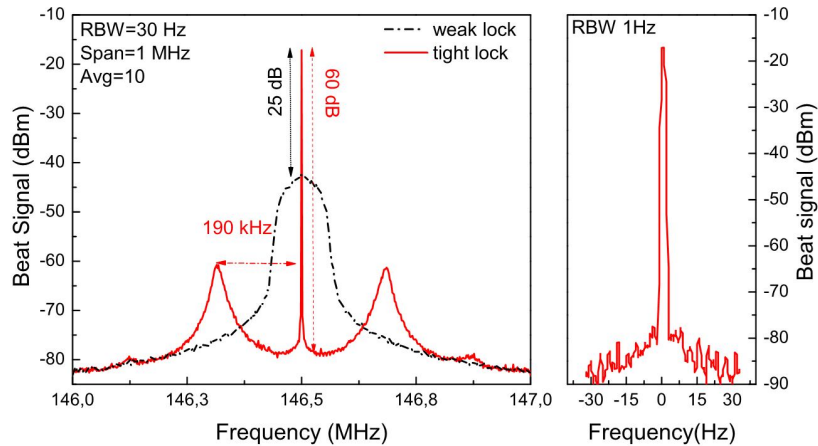

Fig. 2.5.2.2. (a) Example of a beat note between probe and reference lasers under weak (PSD2 deactivated) and tight lock (PSD2 activated) conditions. (b) Beat note under tight lock with higher resolution, characterized by a signal-to-noise ratio of 60 dB, which represents an improvement of 35 dB with respect to the weak lock.

The second setup implementing frequency locking was used to control frequency of the DFB diode laser working at 2.007 µm. It was implemented using optical frequency comb generator (FC1500-250-ULN) as optical reference. As it was mentioned in section 2.4 the frequency corresponding to each component of the comb is defined by the cavity envelop offset frequency f_{ceo}, repetition rate frequency f_{rep} and by the number of the comb tooth n. For the FC1500-250optical frequency comb generator f_{ceo} = 20 MHz and f_{rep} = 250 MHz. The number of the comb component closest to diode laser emission frequency was estimated to be n=598057 at the laser operation conditions used in the current work (laser

frequency corresponds to the center frequency of carbon dioxide line (R(12) line of (20012-00001) band), that is well known). DFB-DL was locked to the nearest in frequency comb component by means of the OFL electronics (Fig. 2.5.2.1, b). The frequency offset between the diode laser and the comb line was locked to the value of 20 MHz. The frequency lock was realized as follows. Portion of the DFB-DL beam and 2-μm part of the frequency comb radiation are focused on a fast photodetector (FPD510) to produce a beat-note signal (Fig. 2.5.2.3), that is filtered, amplified and sent to servo locking (LLE-SYNCRO Locking Electronic Unit). Correction signal from the servo is sent to the laser current driver. Linear frequency scan of the comb repetition rate frequency, and thus, of diode laser is implemented by continuous tuning of RF synthesizer (model RHODE&SCHWARZ SMBV100).
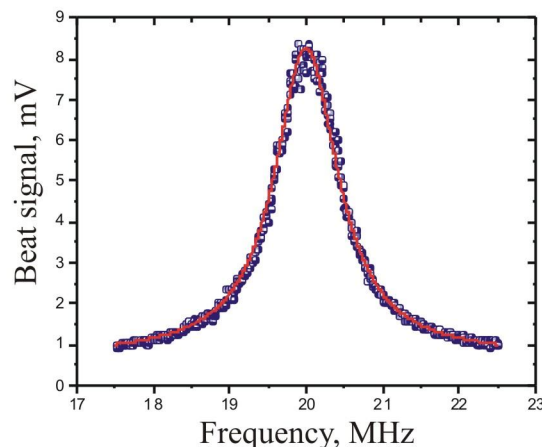

Fig. 2.5.2.3. Example of a beat note signal between DFB-DL and closest in frequency component of the optical frequency comb under lock conditions.

2.6. Doppler Broadening Thermometry

Kelvin is one of the four units of international system SI (kilogram, Ampere, Kelvin, and mole) that must be linked to fundamental constants of Physics (the Planck constant, the elementary charge, the Boltzmann constant and the Avogadro constant). In most physical laws temperature appears in thermal energy together with the Boltzmann constant, thus it can be redefined through it. Several approaches are suggested by the international scientific community. They include acoustic gas thermometry, dielectric constant gas thermometry, Johnson noise thermometry and Doppler-broadening thermometry. The acoustic gas thermometry is based on determination of the k_B from the speed of sound in noble gas, and allows to obtain k_B value with the best relative uncertainty (better than 1 ppm) [59]. Dielectric constant gas thermometry is based upon the Clausius-Mossotti equation and deals with measurements of the electric susceptibility of helium as a function of the gas pressure. It has recently led to a k_B value with a combined uncertainty of 4.3 ppm [60]. Doppler-broadening thermometry offers an independent approach for k_B determination, that is required to confirm previous results. This approach is based on accurate line shape analysis of the recorded molecular (or atomic) absorption line (spectroscopic measurements) aiming at accurate determination of the Doppler width of the line. High precision spectroscopy in combination with a very refined line shape model for the aims of spectral analysis allows one to hope for a progress in redefinition of Kelvin unit.

Doppler broadening thermometry aims to determine the k_B value with a global uncertainty between 1 and 10 ppm. The k_B value can be determined by the reversed equation of Doppler width implementing

38

spectroscopic measurements under the linear regime of laser-gas interaction at the temperature of the triple point of water:

$$k_B = \left(\frac{\Gamma_D c}{v_0} \right)^2 \frac{M}{2 \ln 2 T} \,.$$

(2.28)

It should be mentioned, that for successful application of DBT, several requirements should be satisfied. First of all, it requires isolated spectral line to avoid line interference effects. Then, linear, reproducible low noise spectra with accurate and reproducible frequency scale underneath have to acquired to reduce systematic deviations of obtained value. DBT requires analysis of the recorded spectra with appropriate line shape model, that takes into account all significant effects. During the spectra acquisition the temperature of the absorption cell has to be stabilized at the Triple Point of Water (another alternative is the melting point of Gallium) with a sub-mK stability.

Regarding the choice of DBT molecular target, linear, non-polar molecules (such as CO_2 and C_2H_2) are preferred. Linear structure of the molecules leads to simplified structure of the spectrum and low density of spectral lines simplifying the search for an isolated line. The fact that the molecule does not possess a permanent dipole moment reduces significantly the interactions of the gas with the walls of the gas container. DBT determination of k_B performed on CO_2 [61] and on C_2H_2 [62] exhibits a global uncertainty of 160 and 85 ppm correspondingly. Also H_2O molecule is a good candidate for DBT experiment in the near infrared (NIR) region because of stronger absorption lines. Being a light molecule, H_2O possess a larger Doppler width in comparison with heavier molecules. The DBT experiment on $H_2^{18}O$ molecules [63] gives k_B value with global uncertainty of 24 ppm, that is the best to date result on k_B determination

obtained by using this method. This work is not directly aimed at the DBT determination of k_B. However it can be viewed as a preliminary testing of the existing experimental and theoretical base and approaches for the DBT method by using acetylene.

3. CO$_2$ spectroscopic parameters measurements

3.1. Introduction

One of the particular goals of the study reported in this section was experimental testing of integrated intensity calculation accuracy achieved by modern global *ab initio* method [16,17]. Recent measurements of intensity of 27 vibration-rotation transitions of the P- and R-branch of the (30013)-(00001) vibrational band at 1.6 μm [16] gives uncertainty of 0.3%. Measured line intensity values are in agreement with an accurate theoretical calculation of CO$_2$ [16,17] within declared uncertainty. In respect to CO$_2$ absorption band at 2 μm, experimental investigations of 9 lines [65-67] resulted in line intensity values with estimated uncertainty lower than 0.2%. Line intensity measurements [67] performed only for R(12) line gave value that is in agreement within 0.2% with theoretical value [16,17]. But comparison of the results [65,66] with results of theoretical calculation [16,17] revealed agreement on the level of 1%. To resolve the contradiction an experiment based on new method at 2 μm wavelength was undertaken. It was aimed at highly-accurate determinations of line-intensity factors of a few components of the R-branch of (20012-00001) band. Results are presented in the following section.

3.2. Experimental setup

The experimental set up, which is schematically shown in Fig. 3.2.1.1, is based on a DFB diode laser emitting at 2-μm wavelength, effectively narrowed by exploiting the optical feedback from a V-shaped high finesse optical resonator as described in Section 2.5.1 and similarly to what is usually done in the well known OF-CEAS technique [55,56]. The laser light transmitted through the optical cavity is injected into an isothermal gas cell. Finally, a comb-assisted frequency calibration unit is used to determine the free-spectral range of the resonator, thus providing highly-accurate calibration of the absorption spectra.

3.2.1. The optical resonator

The distributed-feedback diode laser (DFB-DL) with an emission wavelength centered at 2.007 μm is coupled to the high-finesse (~20000) optical cavity. This latter is mounted in a "V" configuration by using three high-reflectivity (R=99.992%, 1-m radius of curvature) mirrors separated by a 52.4-cm long stainless steel spacer. Ringdown time of the cavity is 20.5 μs. The mirrors are fixed to the spacer using adjustable mirror mounts with vacuum o-ring to enable vacuum inside the cavity. The laser light was injected into the cavity through the folding mirror. The cavity provides selective optical feedback to the DFB-DL from the intracavity field when the laser frequency coincides with that of one of the cavity modes. As discussed in section 2.5.1, OF supplies a reduction of the laser linewidth

from about 2 MHz down to about 10 kHz and locking the laser emission to frequency of the cavity mode.
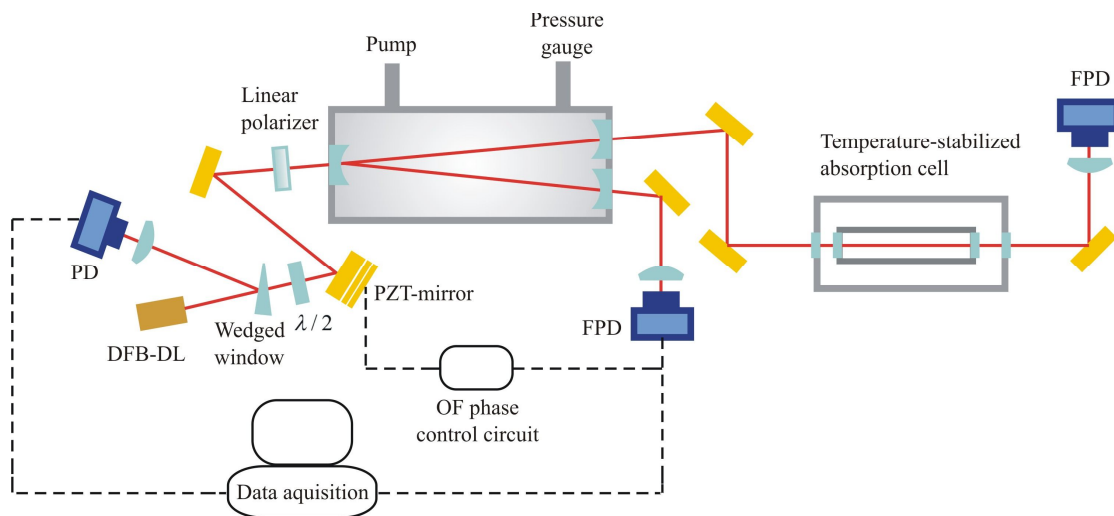

Fig.3.2.1.1. Sketch of the spectrometer. DFB-DL distributed-feedback diode laser, PD - photodetector, FPD - fast photodetector, λ/2 - half wave plate.

Frequency of the laser current is continuously tuned through its driver. The OF locking leads to the stepwise frequency scan of emitted radiation through successive cavity modes. During a single 14-GHz scan, the laser passes through about 100 cavity modes. The radiation is sent to the isothermal cell where the interaction between the light and the CO_2 gaseous sample can be monitored by means of another photodetector, identical to the one monitoring the cavity transmission.

The signals provided by the two FPDs, namely the one coming from the high finesse cavity and from the absorption cell, are acquired using a two channels acquisition board (Gage, model CSE1622) having a 10^6 sample rate and 16 bit of vertical resolution. For each of the two channels, 190000 points can be recorded. A LABVIEW code allows to control the acquisition board, retrieve the maximum value for each of the cavity resonance recorded by the detectors and calculate their ratio in accordance

43

with eq. (2.3). The final result is a CO_2 absorption spectrum, that consists of about 100 points equally separated by the *FSR* of the cavity. Example of the acquired signals and retrieved spectrum are presented in fig. 3.2.1.2.
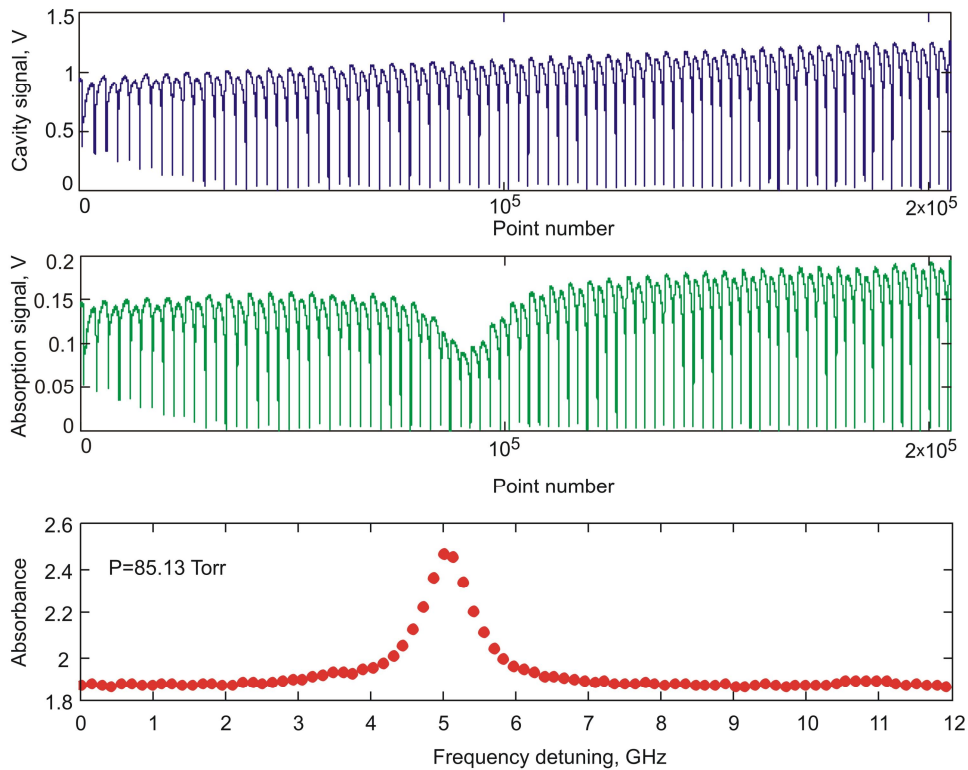
Fig.3.2.1.2. Transmission signal of the V-cavity (1), the signal coming from absorption cell (2), retrieved CO_2 absorption spectrum (3).

3.2.2. The isothermal cell

The absorption cell is mounted inside a stainless steel vacuum chamber, which is equipped with an active temperature stabilization system as described in detail in [65]. Briefly, the cell temperature is measured by a Pt100 precision platinum resistance and kept constant within 0.05 K by means of four Peltier elements driven by a proportional integral derivative controller. This system keeps the gas temperature constant at 296.00 K, with a stability better than 0.01% over 5 min and of about 0.03% over a

whole measurement run (approximately 8 hours). The gas pressure is measured using a 100-Torr MKS capacitance manometer (model 690 A 12 TRA Baratron) having stated by the manufacturer accuracy 0.05 % of the reading. A turbomolecular pump is used to evacuate the cell. A CO_2 gaseous sample with quoted concentration of 99.999 % is used in the experiment.
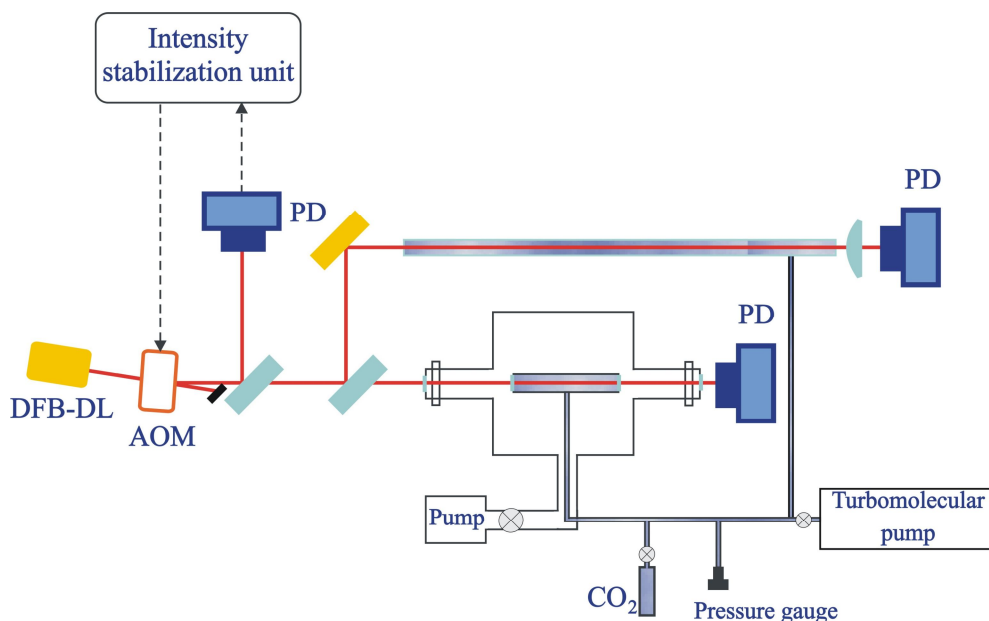
Fig. 3.2.2.1. Sketch of the experimental setup used for absorption cell length determination. DFB-DL stands for distributed feedback diode laser, AOM - acousto-optic modulator, PD - photodetector.

An accurate value for the absorption cell path length is required for further analysis aimed at the line intensity determination. Additional setup for the cell path length measurement was employed. Path length measurement was performed following the approach described in [65, 68]. It exploits comparison of integrated absorbance of CO_2 gas in the absorption cell with integrated absorption in the reference 1-m long cell. Sketch of the setup used for the cell length determination is presented in fig.3.2.2.1. The DFB diode laser, emitting on a single mode at 2.006 µm, is

mounted in a mirror-extended cavity configuration. In this scheme, a partially reflecting mirror, with a 50% reflection coating on one side and an antireflection (AR) coating on the other, provides the optical feedback for line narrowing down to 1 MHz. Laser frequency scans are performed by varying the diode laser injection current and simultaneously changing the external cavity length by means of a piezoelectric actuator. The laser beam is collimated on an acousto-optic modulator AOM that is used as an actuator within a servo loop in order to keep the intensity of the laser beam constant over a laser frequency scan. Driven by a 1 W radio-frequency signal at 80 MHz and properly aligned, the AOM allows to deflect about 70% of the available laser power from the primary beam to the first diffracted order used for the measurements. After being collimated again, the laser beam is divided into three parts by two beam splitters. The first beam impinges on a monitor photodiode, whose output signal is used as the input signal to the servo to control the RF power driving the AOM. The second part is sent to reference 1-m long cell. The remaining portion of the laser beam passes through absorption cell mounted inside a stainless steel vacuum chamber. InGaAs photodetectors are employed to monitor the laser radiation.

The CO_2 absorption spectra of R(12) line were simultaneously recorded in both cells at stable laboratory conditions. Obtained spectra were analyzed using speed-dependent Voigt profile (section 2.2) to obtain integrated absorbance A_C and A_R of the recorded CO_2 line in experimental and reference cells respectively. The procedure was repeated for ten different values of the gas pressure. A linear fit of A_C versus A_R values gives the absorption cell lengths ratio. Taking into account length of

reference cell measured by means of Michelson interferometer [65] and equals to 101.2(1) cm we found L=10.899(60) cm.

3.2.3. The frequency calibration unit

To provide accurate frequency scale underneath recorded spectra, a low-uncertainty measurement of the cavity *FSR* was performed. It was implemented using self-referenced optical frequency comb synthesizer (FC1500-250-ULN), based upon an erbium-doped fiber laser. The repetition rate (f_{rep}) and the carrier-envelope offset frequency (f_{ceo}) were stabilized against the frequency of a Rb-clock. The frequency comb provided a supercontinuum in the wavelength range between 1 and 2.1 μm. The frequency corresponding to each of the comb component is defined by the cavity envelop offset frequency f_{ceo} (equals to 20 MHz), repetition rate frequency f_{rep} (is about 250 MHz) and by the number of the comb tooth *n*: $f_n=f_{ceo}+n·f_{rep}$. The frequency of the *n*-th tooth can be continuously scanned by the tuning of the repetition rate f_{rep}. Another DFB-DL, identical to the one used for the spectroscopic experiment, was locked to the nearest in frequency comb component by means of frequency locking electronics. The frequency of the locked laser f$_{DL}$ is defined as: $f_{DL}=f_n±f_{beat}$, where f_{beat} is frequency offset between the diode laser and the nearest in frequency comb line, that is locked to the value of 20 MHz.

Frequency lock was realized as follows. Portion of the DFB-DL beam and the 2-μm part of the frequency comb supercontinuum radiation were perfectly overlapped using three half-wave plates and a pair of polarizing-cube beam splitters, as illustrated in Fig. 3.2.3.1. The first two half-wave plates, mounted on the two arms before the first cube, were used to

47

maximize optical transmission and reflection, respectively. The third half-wave plates and the second cube adjust the polarization of the two overlapped beams. Hence, a grating is used for optical dispersion and selection of the 2-µm radiation, this latter being focused on a fast fiber-coupled photodetector (Thorlabs FPD510) to produce a beat-note signal, which is filtered, amplified and sent to a servo locking electronics (LLE-SYNCRO Locking Electronics Unit from MENLO). The correction signal from the servo is sent to the laser current driver to actively control the laser emission frequency. Highly accurate and reproducible frequency scans of the diode laser frequency could be performed by tuning the comb repetition rate f_{rep}.
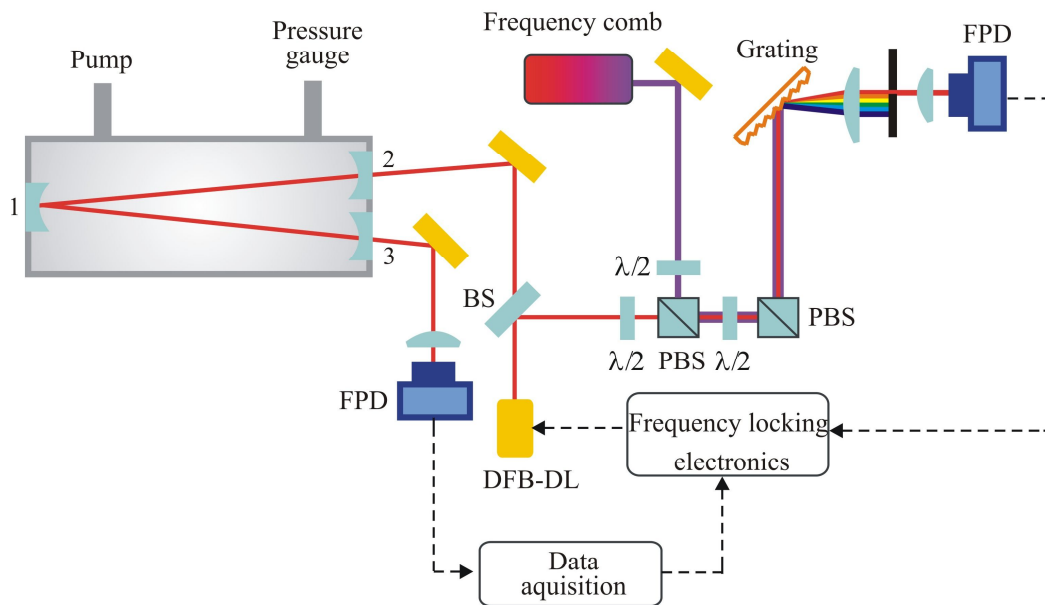

Fig. 3.2.3.1. Sketch of the setup for cavity FSR measurements. DFB-DL distributed-feedback diode laser, FPD - fast photodetector, BS - beam splitter, PBS - polarizing beam splitter, $\lambda/2$ - half wave plate.

The frequency stabilized DFB-DL was coupled to the V - cavity (using the second cavity mirror) and transmission were recorded by tuning f_{rep}. The LABVIEW code performs the frequency scan and acquires the cavity response for each frequency step. Two subsequent cavity modes were recorded and analyzed by means of Airy function (eq. (2.21)), *FSR* was found as difference between their center frequencies. Fig. 3.2.3.2 reports the outcomes of 15 sets of such measurements, each set consisting of 10 repeated spectra. The weighted mean of these values gives a *FSR* of 138.44(3) MHz . The FSR value is in full agreement with the one estimated from the length of the cavity. Possible contribution to the *FSR* uncertainty due a temperature gradient in the cavity spacer can be completely neglected. In fact, a slight variation of the laboratory temperature (within ±2 °C) affects the length of the cavity spacer, thus leading to a variation of the cavity *FSR*. Because of the small temperature coefficient of the cavity spacer, the relative variation of the cavity *FSR* does not exceed 3×10^{-5}.
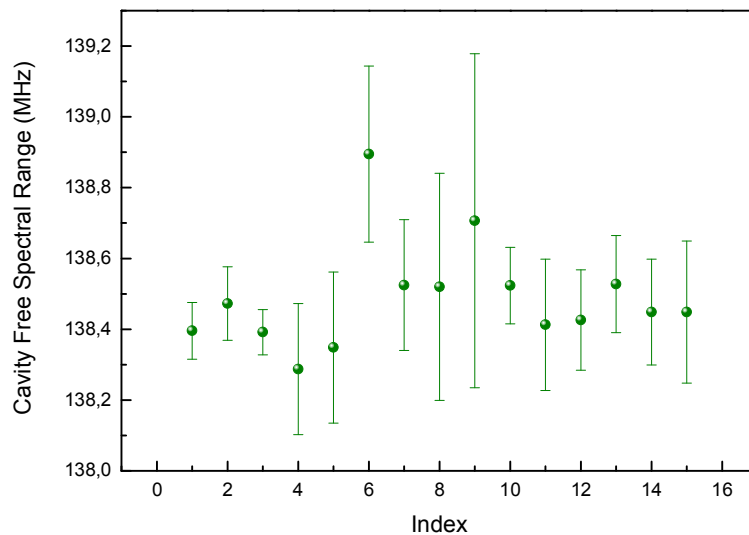

Fig. 3.2.3.2. Determination of the cavity *FSR* splitting frequency. Error bar correspond to one standard deviation of 10 values.

3.3. Data analysis and results

Absorption spectra corresponding to R(2), R(4) and R(6) transitions of the 20012-00001 combination band of carbon dioxide were recorded at room temperature (T≈296 K) at a set of different gas pressures, within the range from 5 up to 100 Torr.

A nonlinear least-squares fit of an experimental profile to a given lineshape model allows one to retrieve the integrated absorbance as well as other resonance profile parameters, including the line center frequency and the collisional width. All the spectra were fitted to the following function:

$$P(v) = (P_0 + P_1 v) \times \exp\left(-\sum_{i=1}^{n} A^i \cdot g^i (v - v_{0i})\right), \qquad (3.1)$$

where P_0 and P_1 are two variable parameters accounting for a possible variation of the laser power, v represents the laser frequency, A and $g(v-v_0)$ are the integrated absorbance and line shape function, while the superscript i (varying from 1 to n) indicates the various lines that are considered, including the probe line and the interfering lines influencing the shape of the probe line. For the aims of the present work $n=3$. Table 3.1 reports spectroscopic data related to the probe and interfering lines. These data are relevant for the spectral analysis.

High-quality determination of the spectroscopic parameters requires a highly accurate and linear frequency scale underneath the acquired spectra and a refined lineshape model accounting for all significantly influencing mechanisms that may affect the observed absorption profiles. In this work, the use of a comb-calibrated cavity-assisted diode laser absorption spectroscopic technique allowed to effectively satisfy the first requirement. The *HTP* model (partially-correlated quadratic speed-dependent hard-collision profile) [43] was used for the lineshape analysis.

As was described in section 2.3, the *HTP* model makes use of the following parameters: the line center frequency v_0, the Doppler width Γ_D, the mean collisional relaxation rate Γ_0, the parameter accounting for the speed dependence of the collisional broadening γ_2, the effective frequency of velocity changing collisions v_{VC} and the η parameter representing the partial correlation between velocity changes and rotational-state changes due to collisions.

Table 3.1. CO_2 lines investigated along with their central frequency and their frequency detuning, Δv, from a pair of interfering transitions [1]. The intensity ratios (I/I_p) of the interfering lines with respect to the probed one are also reported [17].

Probe line	$\tilde{v}_0$ cm^{-1}	Interfering line	Δv (MHz)	I/I_p 10^{-3}
R(6)	4983.091149	21112-01101 R(24)	1600.5019	44.3
		21112-01101 R(25)	-5744.2335	42
R(4)	4981.626214	21112-01101 R(22)	527.3949	65.45
		20012-00001 P(12), $^{13}C^{16}O_2$	-3136.6086	11.2
R(2)	4980.131728	30012-10001 R(30)	774.5138	4.32
		21112-01101 R(20)	-6924.8160	114.24

For each of three probe lines, a global analysis (also known as simultaneous fitting) procedure was applied to the experimental spectra, which were recorded at 20 different gas pressures. As demonstrated in many previous studies (see, i.g, [69]), the advantage of the global analysis is the significant reduction of correlation between varying parameters. The self-broadening coefficient, Γ_0, the γ_2 parameter, the Doppler width, Γ_D, and the η parameter, were shared for each line of the model. The integrated absorbance, the central frequency of the probe line, and the baseline parameters, were retained as varying parameters. The effective frequency of velocity changing collisions was fixed for all the lines at the value

coming from diffusion theory, $v_{VC} = \dfrac{1}{2\pi}\dfrac{k_B T}{MD}$, which was found equal to 1.09 MHz/Torr. As for the parameters of the interfering lines, the frequency detuning from the center of the main line was fixed at the value provided by the HITRAN database [1], while their integrated absorbance was scaled in comparison to that of the probed line according to the intensity ratio reported in [17].
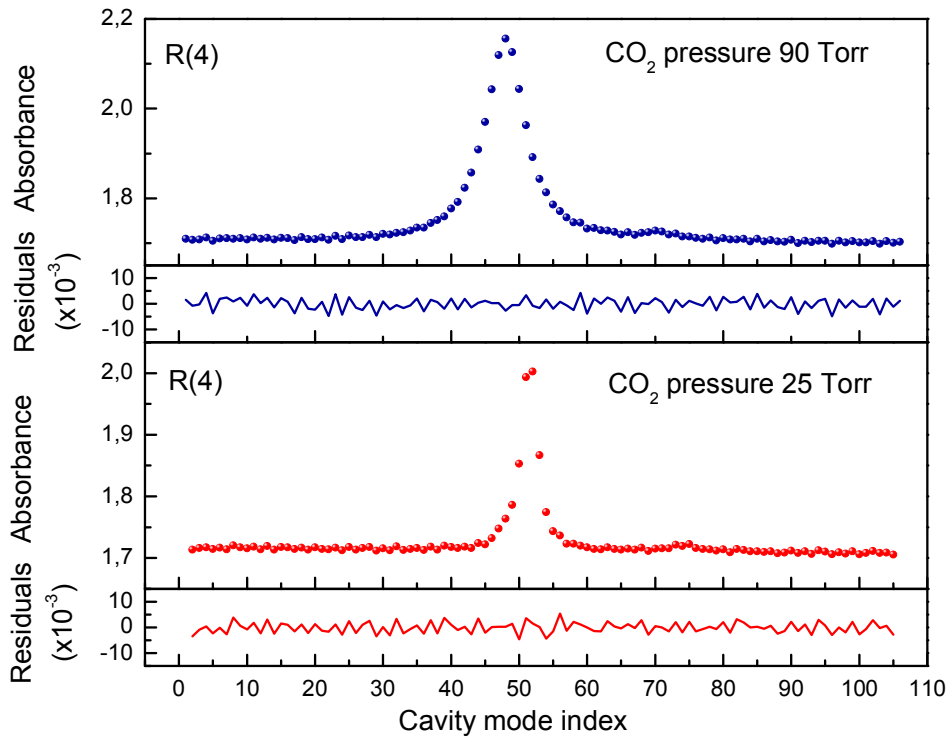
Fig. 3.3.1. Examples of absorption spectra for the R(4) line, along with the residuals resulting from the application of the global fitting approach to a set of 20-pressures spectra, within the range between 5 and 100 Torr.

For each pressure value 100 repeated recordings of the spectrum were acquired which allowed statistical analysis of parameters obtained from the fitting procedure. Result of such fitting for a pair of spectra at different pressures corresponding to the R(4) line, are reported in Fig. 3.3.1. Very

good agreement between the experimental data and the theoretical model is seen, in these two examples. Similar noise-looking residuals was found for all recorded spectra. The root-mean-square value of the residuals amounts to about 2×10^{-3} (absorbance units) presenting the experimental noise. No clear systematic structures could be evidenced in the residuals, at any pressure. This demonstrates the capability of the *HT* profile for adequate modeling the absorption spectra over the entire pressure range used in this experiment.

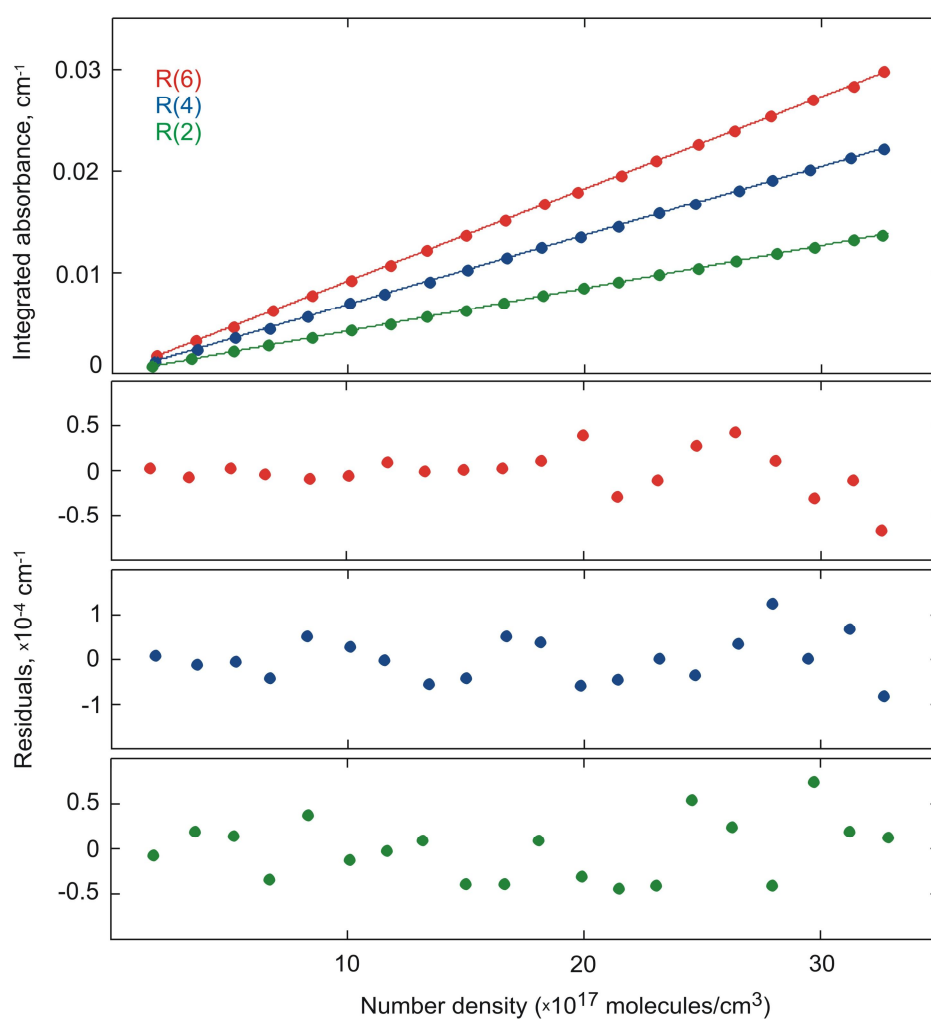Fig. 3.3.2. Plot of the integrated absorbance as a function of the molecular number density.

Fig. 3.3.2 represents sets of retrieved values of the integrated absorbance (resulting from the application of the global fitting approach) as a function of the molecular number density, for the R(6), R(4) and R(2) lines. The gas pressure, temperature, and purity, as well as the isotopic composition of the sample gas were taken into account in the number densities calculation. Each point results from the statistical analysis of 100 values, yielding the mean value and the standard deviation. The experimental points were fitted to a straight line by using a weighted total least-squares linear regression [70], so as to consider the uncertainties on both the absorbance and the number density. These experiments were repeated, twice for each of the investigated lines, in different days. Thus the linestrength S was retrieved from a weighted mean of two different set of measurements.

Table 3.2. Measured line intensities with their global uncertainty in comparison with values from databases [1,3], results from recent theoretical calculations [17] and from past experimental studies [65,66]. Intensity values are given in $\times 10^{-22}$ cm/molecule and following the HITRAN convention are rescaled to the isotopic $^{12}CO_2$ natural abundance, namely 0.9842 [1].

Line	R(6)	R(4)	R(2)
Present work	8.355±0.014	6.235±0.012	3.844±0.009
Ab-initio calculations [17]	8.348	6.210	3.822
Relative deviations (%)	0.08	0.40	0.57
HITRAN values [1]	8.133	6.049	3.722
GEISA values [3]	8.309	6.182	3.805
Values from Ref. [65]	8.305±0.013	6.229±0.008	3.789±0.006
Values from Ref. [66]	8.263±0.013	6.187±0.009	3.780±0.006

Excellent agreement is found between the line and the experimental points. The slope of the best-fit line provides the quantity *SL*, from which the line intensity factor can be determined, using the value of the absorption pathlength (Section 3.2.2). As expected, the intercept of the best-fit line is well consistent with zero within the experimental uncertainty.

The measured line intensities are given in the Table 3.2, along with values resulting from *ab-initio* calculations [17], values from databases [1,3], and values from previous experimental studies [65,66]. The uncertainties of the measured line intensity factors include both purely statistical (corresponding to 1-σ) and caused by possible systematic uncertainties. The fourth column gives the relative deviations between the present measurements and aforementioned *ab-initio* calculations. The level of agreement is very satisfactory, the mean relative deviation being 0.35%. It should be noted that such the deviation increases as J is lowered, probably because of the decreasing signal-to-noise ratio in the recorded spectra. Furthermore, the new experimental values show a relative deviation from those of Ref. [65] of 1.1 %, -0.77% and 1.66% respectively for the R(6), R(4) and R(2) lines. Similarly, the relative deviations from the data of Ref. [66] amount to 0.6%, 0.1% and 1.43%. Therefore, it appears that the data from past experiments are less accurate than it was expected. This could be partly due to the inadequacies of the line shape models used in past works to perform the spectral analysis [65,66]. Another source of the deviation can be ascribed to the pressure gauges, which were used for the former measurements [65,66]. A further remark comes from the comparison with the databases. It turns out that the level of agreement is much better for the GEISA values, rather than the HITRAN 2012 database.

In particular, the mean deviation amounts to 0.81% for GEISA and 2.94% for HITRAN 2012. It should be noted, that theoretical transition intensities from Ref. [17] are included in the recently-released 2016 edition of the HITRAN database [71].

As far as the uncertainty budget is concerned, it is useful to remember that the evaluation of so-called type A uncertainties is based on any valid statistical method for treating data, while type B uncertainties (including systematical deviations) are inferred from scientific judgment or other information concerning the possible values of the quantity. The type A uncertainty could be directly inferred from the weighted mean of values resulting from linear fits similar to that of Fig. 3.3.2. As stated above, in the linear best-fit procedure we took into account the uncertainty on the integrated absorbance as well as the one on the molecular number density. In particular, the former results from the statistical analysis of 100 values for each pressure, as retrieved from the global fitting procedure. The latter comes from the combination of two contributions, of the type A and type B, related to the temperature measurement (0.02%) and to the accuracy of the pressure reading (0.054%), respectively. It must be noted that the uncertainty on the gas pressure also includes a 0.02% contribution originating from the measurement of the isotopic composition of the gas sample (determined by means of conventional isotope ratio mass spectrometry). Finally, from the weighted linear fits, an overall type A uncertainty in the range between 0.15% and 0.20% was quoted, depending on the investigated absorption line.

Type B contributions can be ascribed to (i) the optical path length, (ii) the detector's nonlinearity, (iii) the influence of the line-shape model, and (iv) the *FSR* uncertainty. The overall component associated to the optical

path length resulted to be 0.06%, also in this case a combination of a statistical uncertainty (0.055%) and a type B uncertainty (0.019%) associated to the length of the reference cell.

Regarding the detector nonlinearity, we assumed that the performance of extended-wavelength InGaAs photodiodes was similar to standard-type InGaAs detectors, which show a linearity within 0.04% (at one standard deviation) over the photocurrent range from 10^{-7} to 10^{-4} A [72]. In order to quantify its influence on linestrength determinations, we adopted the following procedure: after simulating "nonlinear" absorption spectra, we did the spectral analysis and determined the integrated absorbance, which was compared to the expected one. We found an average relative difference (over the simulated pressure range) of about 6×10^{-4}. In a very pessimistic view, the simulated nonlinearity was considered in the form of a frequency-dependent second-order polynomial added to the vertical scale of each simulated spectrum so that the relative deviation between original and distorted spectra was 0.04%.

In order to quantify the influence of the adopted line shape model, we numerically simulated CO_2 spectra (in the pressure range 5-100 Torr), in coincidence with the R(6) line, assuming that the line profile is given by a partially-correlated speed-dependent hard collision model with a hypergeometric dependence on the absorber speed for both pressure broadening and pressure shifting parameters (pcSDHC-hg). Then, the application of the global fitting procedure, based on the use of the *HTP* model, to the set of simulated spectra showed that the systematical deviation between retrieved and expected linestrength values was negligible. This is expected on the basis of the outcomes of paper [72], where despite the strong differences between *HTP* and pcSDHC-hg models

in the physical interpretation of the narrowing mechanisms, the determination of the absorbance resulted to be quite robust, regardless of the choice of the form used to represent the speed dependence.

The last source of type B uncertainty can be ascribed to the cavity *FSR*. Since the free-spectral-range enters into the frequency scale calibration, its uncertainty may influence the accuracy of linestrength determinations. To this end, the overall spectral analysis (global fitting plus weighted linear fits) was repeated adopting two different *FSR* values, at the two edges of the interval $FSR \pm \sigma_{FSR}$, where σ_{FSR} is the statistical uncertainty of the *FSR* determination (namely, 0.03 MHz). So doing, we include a 1-σ systematic component of 0.03 % in the uncertainty budget for the linestrength determinations.

To summarize, the complete uncertainty budget leads to a 1-σ global uncertainty of 0.17%, 0.19% and 0.23% respectively for the R(6), R(4) and R(2) lines. The line shape parameters resulting from the application of the global-fitting approach are presented in Table 3.3. The values for the partial correlation parameter sound reasonable, being close to the ones retrieved in [73] for some components of the R-branch of the (30013)-(00001) band, using the same line shape model. The quadratic speed-dependence parameter, γ_2, is consistent with an interaction potential of the form C/r^q, with the exponent q roughly varying between 5 and 7, the former being typical of a quadrupole-quadrupole interaction, the latter occurring for a quadrupole-induced dipole force. As for pressure broadening coefficient Γ_0, obtained values are greater than those of the HITRAN database [1]. This difference can be explained by the fact, that in the HITRAN database [1] provides pressure broadening coefficients supporting Voigt profile (eq. (2.8)). Similar difference was observed also in other works (for example

[74]), in which speed dependences of the relaxation rates were taken into account.

Table 3.3. Line shape parameters (Γ_0, Γ_2, η) measured in the present work. The pressure broadening coefficient is given in terms of a half-width at half maximum.

Line	Γ_0 (cm^{-1}/atm)	γ_2	η	Γ_0 (cm^{-1}/atm) HITRAN [1]
R(6)	0.1162±0.0003	0.195±0006	0.23±0.02	0.114±0.002
R(4)	0.1206±0.0005	0.201±0.008	0.19±0.04	0.116±0.002
R(2)	0.1229±0.0006	0.174±0.012	0.17±0.06	0.119±0.002

3.4. Conclusion

A new laser absorption spectroscopic method was applied to measurements of carbon dioxide line intensities at the wavelength region near 2-μm. The advantages of this method lie in narrow spectral width of the DFB diode laser, that is used to probe CO_2 vibration-rotation transitions, and in highly-accurate frequency scale underneath the recorded absorption spectra. Narrowing of the laser spectral width to the kHz level was attained using optical feedback from the high-finesse V-shaped optical cavity. The frequency calibration unit based on a self-referenced optical frequency comb synthesizer provides highly-accurate frequency scale.

Absorption spectra corresponding to three CO_2 vibration-rotation transitions of the (20012)-(00001) band (namely R(2), R(4) and R(6)) were recorded. A global fitting approach, with the use of Hartmann-Tran profile as line shape model, has been adopted for the simultaneous analysis of a manifold of experimental spectra across the pressure range between 5 and 100 Torr. This procedure allows to reduce statistical correlation between free parameters by sharing some of them within sets of spectra.

The global uncertainty for the linestrength determinations was found to vary from 0.17% to 0.23%. The agreement between the measurements and *ab initio* calculations resulted to be at the level of 0.35%, which is well within the estimated theoretical uncertainties. This comparison provides an important demonstration of the validity of the theoretical procedure for determining CO_2 line intensities also for the 2-μm wavelength region.

4. C$_2$H$_2$ spectroscopic parameters measurements

4.1. Introduction

Acetylene is an important trace constituent in the atmospheres of Earth and other planets. It was found in the atmosphere of Saturn's satellite Titan. Quantitative information on C$_2$H$_2$ densities is extremely important in several research fields, such as combustion science, astrophysics, and Earth and planetary atmospheric chemistry. The density retrieval from C$_2$H$_2$ spectra requires accurate knowledge of line positions, integrated intensities, broadening and shifting coefficients.

In the last few years, spectroscopic data regarding the near-infrared spectrum of acetylene have been considerably enriched, especially in six different spectral regions, namely, around 3, 2.2, 1.9, 1.7, 1.5, and 1.4 μm [75]. Many efforts have been made in this field, using well-consolidated spectroscopic techniques, such as high-resolution Fourier transform spectrometry [76], direct laser absorption spectroscopy [77], cavity ring-down spectroscopy [78,79], and spectroscopic techniques assisted by the technology of optical frequency combs [80,81]. However, in the majority of these studies, the Voigt profile (*VP*) has been adopted for the spectral analysis . The more accurate line shape model adopted in this work (*HTP*) has been successfully applied just for P$_e$(11) line of the $\nu_1 + \nu_3$ band at 1.5 μm [82].

In this work the P$_e$(14) line of the $2\nu_3 + \nu_5^1$ band of C$_2$H$_2$ was investigated, using an absorption spectrometer based upon a pair of phase-locked extended-cavity diode lasers, at pressures ranging between 3 and 30 Torr and at the constant temperature of the triple point of water (273.16 K). The spectrometer allowed to perform highly accurate and reproducible

frequency scans around a given center frequency. This feature, in conjunction with the linearity of the detection chain, made it possible to avoid any instrumental distortion in measuring absorption line shapes, reaching an experimental accuracy limited by only the noise level. Using the *HTP* model, the line intensity, self-broadening and self-shifting coefficients were retrieved with a relative uncertainty of about 0.22, 0.13, and 0.18%, respectively. Analysis of the recorded C_2H_2 spectra allowed also to retrieve Boltzmann constant k_B with global uncertainty of 40 ppm using the DBT approach.

4.2. Dual-laser spectrometer at 1.39 um

The dual-laser spectrometer, schematically reported in Fig. 4.2.1, essentially consists of an extended-cavity diode laser (namely, the probe laser) with an emission wavelength in the range between 1.38 and 1.41 μm, a frequency stabilization and control unit (including a reference laser), an intensity stabilization feedback loop, and an isothermal cell.
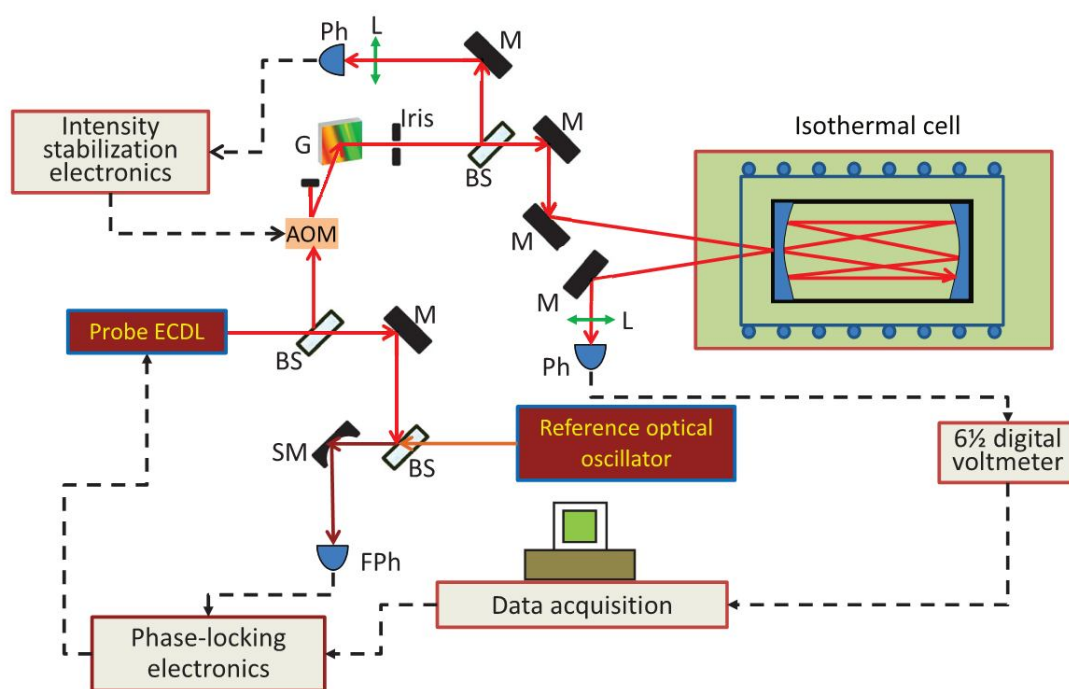
Fig. 4.2.1. Sketch of the dual-laser spectrometer. BS, beam splitter; M, mirror; SM, spherical mirror; G, grating; L, anti-reflection coated lens; AOM, acousto-optic modulator; Ph, InGaAs photodiode; FPh, fast photodiode.

The probe laser (PL) was phase locked to the reference laser (RL) by using the phase-locking electronics that is described in detail in section 2.5.2. The RL was an optical frequency standard based on noise-immune cavity-enhanced optical heterodyne molecular spectroscopy (NICE-OHMS) [83]. More specifically, the emission frequency of an extended-

cavity diode laser (ECDL) was actively stabilized against the center of a sub-Doppler $H_2^{18}O$ line, observed under optical saturation conditions in a high-finesse resonator [57]. NICE-OHMS provides a dispersion signal without dithering the optical cavity, which is employed as an error signal. The emission line width of the RL was found to be about 7 kHz (full width at half maximum) for an observation time of 1 ms [58].

Amplitude variation in the background baseline, that could produce systematic deviations, is essentially removed by implementing an intensity control feedback loop which effectively compensates for any power variation of the probe laser. Part of the primary beam passes through acousto-optic modulator (AOM), that is used as actuator within a servo loop to keep the intensity of the laser beam constant over the laser frequency scan. Driven by a 1 W radiofrequency signal at 80 MHz AOM deflects about 70% of the laser power beam to first diffracted order. Part of the transmitted beam is focused to a monitor PD, whose output signal is used as input signal to the servo to control the radiofrequency power driving the AOM. The other part is sent to the isothermal cell. Two identical ultralow-noise 10-kHz bandwidth preamplified InGaAs photodiodes (New Focus, model 2011-FS-M) were used to produce the reference signal and to monitor the power on the output of the isothermal cell. Relative intensity instability of the order of 10^{-4} was achieved.

Laser-gas interaction takes place inside an isothermal cell, actively stabilized at the temperature of the triple point of water. It consists of a spherical, Herriott-type, multiple reflection cell with a maximum path length of 12 m in a volume of about 400 cm^3. The cell is made from in the stainless steel, with electro-polished inner and outer cavity surfaces. Temperature control and measurements were performed by using a pair of

capsule-type standard platinum resistance thermometers (SPRTs, Hart Scientific, model 5686). The two SPRTs are placed inside the cylindrical spacer, into two holes drilled in the opposite sides of the cell. The displacement of the SPRTs sensing elements allowed for the evaluation of the maximum temperature gradient, since they are positioned in both radial and axially opposite positions. SPRTs were calibrated at the Italian Institute for Research in Metrology in the temperature interval between the triple point of mercury and the indium freezing point. Temperature stability (as determined over one full day at the temperature of the triple point of water) was found to be at the level of 0.1 mK, while temperature homogeneity was better than 1 mK. These extraordinary performances were ensured by using the system [84], essentially made of two cylindrical chambers, one inside the other, the multipass cell being housed inside the inner one. In order to obtain acoustic and thermal insulation from the outside environment, the two chambers were kept under vacuum conditions. Two independent temperature stabilization stages were used: an auxiliary thermostat and a fine heating control, the former acting on the inner chamber (exploiting the circulation of a thermal fluid), the latter on the multipass cell (through a constantan heater wire, uniformly wrapped around the cell body).

A digital voltmeter, with six and half-digit resolution (Agilent, model 34401A), connected to a personal computer through a USB-GPIB board, was used to measure the transmitted signals. Highly linear, accurate, and reproducible frequency scans of the PL around a given center frequency were implemented by continuously tuning the RF offset frequency. A Labview code was developed to perform the step-by-step frequency scan and to acquire, for each step, the transmitted signal.

The gas pressure was measured by means of a 100-Torr capacitance manometer (model VCMT12TDA from Varian), with a stated accuracy of 0.25% of the reading. A turbomolecular pump was used to periodically evacuate the isothermal cell and create high-purity conditions. The acetylene sample was in a commercial bottle with a quoted concentration of 99.6%. Unfortunately, the manufacturer did not provide the uncertainty for the gas purity. In the data analysis, it was conservatively set to 1%. The natural abundance, namely, 97.7599% of $^{12}C_2H_2$ was assumed regarding the isotopic content of the sample.

4.3. Line shape parameters determination

In this work the $P_e(14)$ line centered at frequency 7183.39 cm^{-1} corresponding to C_2H_2 rovibrational band $2v_3+v_5$ was investigated. Reference laser was stabilized against water vapor $H_2^{18}O$ line that corresponds to $5_{5,0} \rightarrow 5_{5,1}$ transition of (101-000) vibrational band, thus providing frequency separation of 5.87 GHz from the center of the acetylene line. The transmission spectra were recorded at 273.160(1) K as a function of the gas pressure, which was varied between 3 and 30 Torr. In total 220 spectra corresponding to 11 pressures were recorded. Typical examples of the spectra are presented in figure 4.3.1.
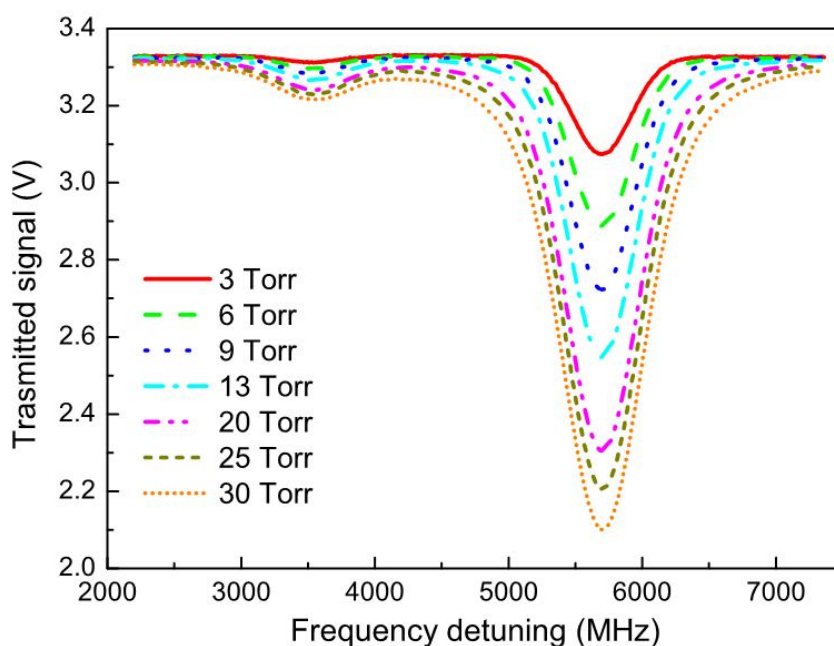

Fig. 4.3.1. Examples of absorption spectra of the $P_e(14)$ transition of C_2H_2 acquired as a function of the gas pressure. On the horizontal axis the frequency offset of the probe laser with respect to the reference one is reported.

Weak absorption line at the low-frequency side of the scan, is not reported in the HITRAN database [1], but according to the line list of [78] the interfering line belongs to $^{13}CH^{12}CH$ molecule.

Laser scans were 5160 MHz wide and resulted from 1032 steps of 5 MHz each. All the spectra were fitted to the following function:

$$P(v) = (P_0 + P_1 v) \times \exp(-A^P \cdot g^P (v - v_0^P) - A^I \cdot g^I (v - v_0^I)), \quad (4.1)$$

where the parameters P_0 and P_1 account for a possible residual variation of the incident power, v and v_0 represents the current frequency and unshifted position of the line in the units of frequency detuning from RL, and A^P and $g^P(v - v_0^P)$ are the integrated absorbance and the line-shape function of the probed line, respectively. Similarly, the quantities denoted by the superscript I refer to the $^{13}CH^{12}CH$ neighboring line. The HTP model was adopted for the line-shape function. In the global fitting procedure, P_0 and P_1 and the integrated absorbance A^P were free parameters of individual spectra, while v_0^I, v_0^P, pressure broadening parameters Γ_0^I and Γ_0^P, and center frequency shifting parameters δ_0^I and δ_0^P were shared across spectra in the whole pressure range, the quantities Γ_0 and δ_0. The integrated absorbance of the neighboring line, A^I, was constrained to be proportional to A^P, the proportionality factor being a free parameter, also shared among the various spectra. The two Doppler widths, Γ_D^I and Γ_D^P, were fixed at the calculated values. The remaining line shape parameters, β_{VC}, (the velocity-changing collision rate), γ_2 (speed dependent broadening) and δ_2 (speed dependent shifting) were set equal for the two lines and shared among the spectra.
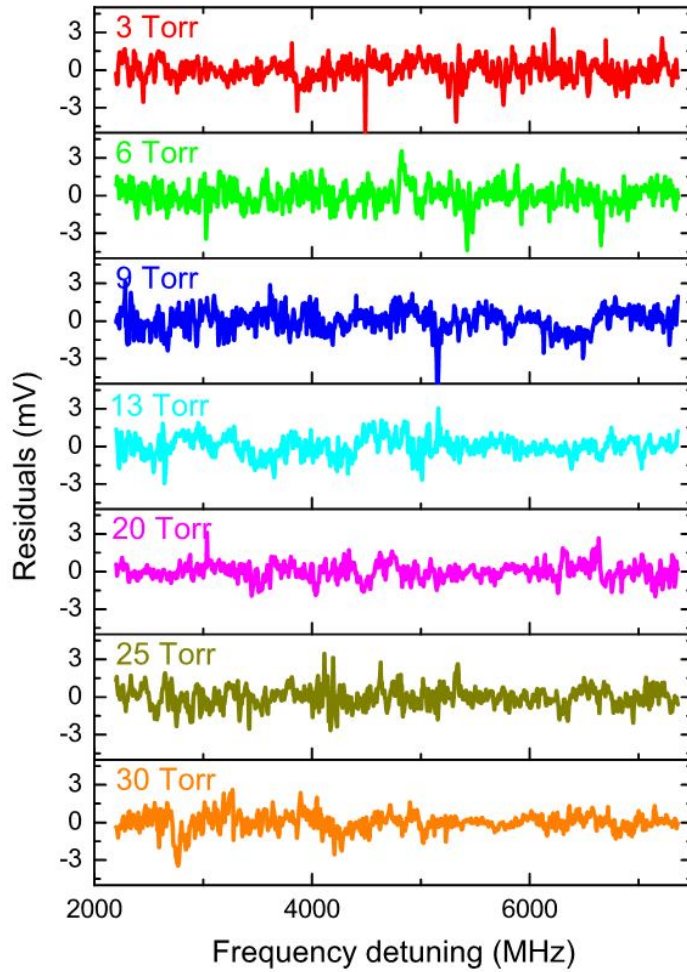
Fig. 4.3.2. Residuals resulting from the nonlinear least-squares global fit of Eq. (4.1), for all the spectra of Fig. 4.3.1.

Figure 4.3.2 shows the residuals resulting from the application of the global-fitting procedure to the seven spectra of Fig. 4.3.1. The root-mean-square of the residuals ranging from 650 to 900 μV, mostly limited by the experimental noise, indicate the excellent agreement between the experimental data and the theoretical model. In the experimental conditions, for a laser power of 50 μW impinging on the detector, we could calculate a voltage shot-noise limit of about 25 $nV/\sqrt{Hz}$. This value is almost a factor 30 000 lower than the noise observed in the absorption spectra. A possible source of the noise could be ascribed to the residual

69

laser power fluctuations not properly compensated by the intensity stabilization loop. Extra noise could be also introduced either from unwanted electrical pick-up or from residual mechanical vibrations converted in spurious laser power fluctuations. However, no clear structures or systematical variations could be evidenced. Also, there was no dependence on the gas pressure, a circumstance that demonstrates the capability of the *HTP* of modeling the absorption spectra in the entire pressure range of this experiment.

Table 4.3.1. Spectroscopic parameters obtained at T = 273.16 K (first line) and rescaled at T_0 = 296 K (second line) for comparison with previous works. The quantity Γ_0 was rescaled to T_0 using the equation $\Gamma_0(T_0) = \Gamma_0(T) \cdot (T/T_0)^n$, n = 0.75 [1]. Overall uncertainties, in parentheses, correspond to one standard deviation.

$S \cdot 10^{-23}$ cm/molecule	Γ_0 cm^{-1}/atm	δ_0 cm^{-1}/atm	γ_2	δ_2	β_{VC} cm^{-1}/atm
1.584(3)	0.1602(2)	-0.006746(12)	0.1217(2)	0.2140(6)	0.03058(7)
1.555(3)	0.1508(2)				0.02937(7)
S = 1.551· 10^{-23} cm/molecule [1]					
S = 1.538· 10^{-23} cm/molecule [75]					
S = 1.508· 10^{-23} cm/molecule [76]					

The measured parameters are reported in Table 4.3.1. Data from previous studies [75,76], and from the HITRAN database [1], have been also listed for comparison. The transition strength value, S, reported in HITRAN for the $P_e(14)$ line has a relative uncertainty of 2–5%, and one reported in [75] has estimated accuracy in the range between 3 and 5%. The latter one was obtained using a multispectrum fitting procedure based on the use of the Voigt profile aiming to determine the absorption

coefficients of the lines, while the self-broadening coefficients were fixed at some theoretically calculated values and the pressure shifting effect was set to zero. Obtained transition strength value S is slightly shifted towards a higher value with respect to the others, even being in good agreement with the HITRAN value [1] and with that of [75]. In contrast, the line intensity factor reported in [76] is significantly ($\sim$ 3%) different from value obtained in the current work, the relative difference is a factor of 30 bigger than the quoted uncertainty. Self-broadening coefficient value Γ_0 presented in the HITRAN database [1]equals to 0.141 cm^{-1} /atm, with a relative uncertainty in the range 2–5%. It was obtained by theoretical extrapolation from lines belonging to 15 hot bands involving the $v_4 = 1$ and $v_5 = 1$ vibrational levels [85], is 0.141 cm^{-1} /atm, with a relative uncertainty in the range 2–5%. After rescaling the measured value to the reference temperature $T_0 = 296$ K using temperature-dependent exponent for Γ_0 of 0.75 (as it is recommended in [1]), a self-broadening coefficient was found to be about 6% larger than the one reported in HITRAN, that is expected, because HITRAN database supports Voigt line shape profile, that leads to lower Γ_0. On the other hand, a good agreement with the value reported in [76], $\Gamma_0 = 0.1522(2)$ cm^{-1}/atm (this latter was measured at 295 K) was obtained.

The determination of the line intensity, S, requires the knowledge of the absorption path length, L, and the conversion of the C_2H_2 pressures in absorbing molecule number density. The measurement of the path length inside the multiple reflection cell was carried out following the procedure described in detail in [68]. The procedure is similar to the CO_2 cell length calibration presented in section 3.2.2 and is based on comparison of observed absorption with a result of the use of 1-m-long reference cell (is not shown in Fig. 4.2.1 for the sake of simplicity) at the same

thermodynamic conditions. The spectral analysis was performed by using the speed-dependent Voigt profile, in order to retrieve the integrated absorbance in the multiple reflection cell, A_{MRC}, and in the reference cell, A_{REF}. These measurements were repeated for ten different values of the gas pressure, in coincidence with the Pe(14) line. A linear fit of the A_{MRC} data as a function of A_{REF} (shown in Fig. 4.3.3) provides the ratio of cell lengths. The multipass cell length $L = 849$ (1) cm was found taking into account the length of reference cell 101.2(1) cm measured by means of Michelson interferometer [65]. The combined uncertainty resulted from a statistical contribution of 0.07% and a systematic component of 0.1%.
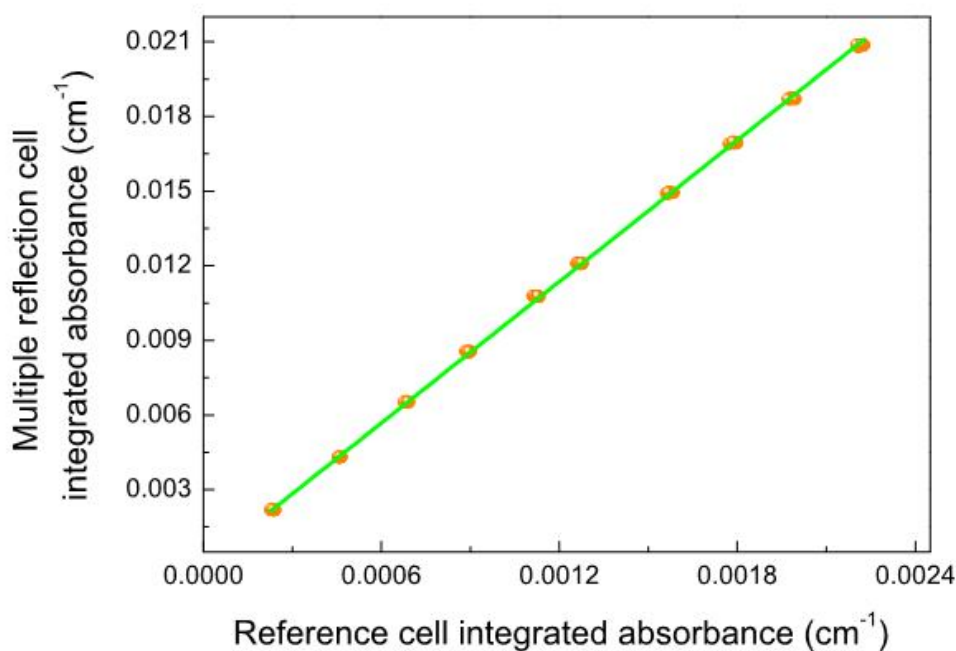

Fig. 4.3.3. Plot of the integrated absorbance in the multiple reflection cell as a function of the same quantity in the reference cell. The slope of the best-fit line is equal to the ratio between the multipass and reference cell lengths.
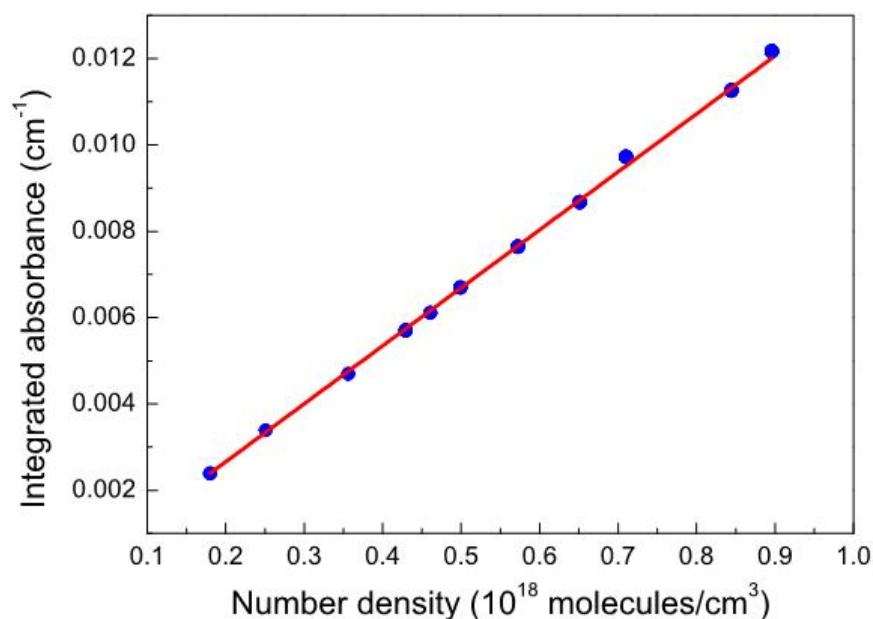
Fig. 4.3.4. Plot of the molecular number density versus the integrated absorbance. The best-fit line exhibits an excellent agreement with the experimental points. The slope of the line provides the quantity SL. The dispersion of the points, for each pressure, is not visible, being much smaller than the size of the points.

Fig. 4.3.4 presents the data used for the $P_e(14)$ transition strength determination. In calculating the number densities, the gas purity and the gas temperature were taken into account. Furthermore, the natural isotopic abundance for $^{12}C_2H_2$ molecules was assumed (as given in the HITRAN database). For each of 11 pressure, 20 repeated measurements were performed. The experimental points (220 in total) were fitted to a straight line by using a weighted total least-squares linear regression [86], so as to consider the uncertainties on both the absorbance and on the number density. The perfect agreement between the data points and the linear fit of Fig. 4.3.4 was due to two main factors: the very high experimental reproducibility in recording absorption spectra, ensured by the repeatability of the frequency scan, and the good performances of the temperature

stabilization system. Since the HITRAN value refers to the temperature T_0=296 K, it was necessary to rescale the retrieved $S(T)$ value to the reference temperature, using the following equation:

$$S(T_0) = S(T)\frac{Q(T)}{Q(T_0)}\left[1-\exp\left(-\frac{hcv_0}{k_B T_0}\right)\right]\times\left[1-\exp\left(-\frac{hcv_0}{k_B T}\right)\right]^{-1}\times$$
$$\times\exp\left[-hc\frac{E}{k_B}\left(\frac{1}{T_0}-\frac{1}{T}\right)\right]$$

(4.3.2)

where h being the Planck constant, E the energy of the lower level of the transition in cm^{-1}, and Q the total internal partition function calculated by means of the well-known polynomial approximation [87].

Table 4.3.2. Uncertainty budget (in terms of relative contributions, corresponding to one standard deviation) for the line intensity determination.

Contribution	Type A	Type B
Linear fit	0.17%	
Path length	0.07%	0.1%
Linearity of frequency scale		Negligible
Detector's nonlinearity		0.03%
Laser emission linewidth		Negligible
Partition function		0.04%
Temperature	Negligible	0.0012%
Total uncertainty	0.22%	

The complete budget of uncertainties for the line intensity determination is reported in Table 4.3.2. Type A and type B uncertainties are distinguished. Type A uncertainty is due to the statistical uncertainty of the linear fit of Fig. 4.3.4, which, in turn, takes into account the type A uncertainty on the integrated absorbance and the type B uncertainty of the

molecular gas density. This latter was related to the pressure measurement, the uncertainty of which was estimated as 1% (a combination of the accuracy of our pressure gauge and the uncertainty on the sample purity of the gas sample, and the former is much less than the latter). In contrast, the contribution to the uncertainty due to the temperature (type A and B) was completely negligible, being at the level of 1×10^{-6}. From the weighted linear fit, an overall type A uncertainty of about 0.17% was obtained. Type B contributions are ascribed to (i) the optical path length, (ii) the detector's nonlinearity, (iii) the linearity of the frequency scale, (iv) the laser emission width, and (v) the partition function. The overall component associated to the optical path length resulted in 0.12% (a combination of 0.07 and 0.1% of type A and B uncertainties, respectively). Regarding the detector nonlinearity, it is useful to recall that InGaAs photodiodes show a linearity within 0.04% (at one standard deviation) over the photocurrent range from 10^{-7} to 10^{-4} A [72]. In order to quantify its influence on the integrated absorbance, we adopted the following procedure: after simulating "nonlinear" absorption spectra, we did the spectral analysis and determined the integrated absorbance, which was compared with the expected one. We found an average relative difference (over the simulated pressure range) of 3×10^{-4}. It is worth noting that the nonlinearity was considered in our simulations in the form of a frequency-dependent second-order polynomial added to the vertical scale of each simulated spectrum so that the relative deviation between original and distorted spectra was 0.04%. Similarly, the analysis of numerically simulated spectra showed that the systematical contributions due to the laser linewidth and to the linearity of the frequency scale could be neglected. In fact, thanks to the phase locking electronics, the spectral purity of the PL was at the level of a few kHz, namely, at least

a factor 10^{-5} smaller than the width of the absorption line in the worst case. On the other hand, measuring the difference between the frequency of the RF synthesizer and that of the beat note, the nonlinearity of the frequency scan was found to be smaller than one part over 10^8 for a 5-GHz scan. Finally, a further source of type B uncertainty could be ascribed to the partition function. Since $Q(T)$ contributes during the rescaling of S to the reference temperature T_0 [Eq. (4.3.2)], its uncertainty must be properly taken into account. Following the outcomes of [87], it was found that this additional contribution amounts to 0.04%. The complete uncertainty budget leads to an overall intensity measurement uncertainty of 0.22%.

4.4. Application to Doppler Broadening Thermometry

The best result ever obtained by using an optical method for Boltzmann constant determination was obtained implementing DBT on $H_2^{18}O$ molecules at the temperature of the triple point of water [63]. This approach allowed to reach global uncertainty of 24 parts over 10^6 of k_B determination, meanwhile the new definition of the unit kelvin requires accuracy of 1 part per million.

Being a non-polar and linear molecule, C_2H_2 offers some important advantages for DBT in comparison to water. In particular, the fact that the molecule does not possess a permanent dipole moment reduces significantly the interactions with the walls of the gas container. Moreover, despite the relatively large number of vibrational modes (five in total, namely, the symmetric C-H stretch, the symmetric C-C stretch, the antisymmetric C-H stretch, the antisymmetric bend, and the symmetric bend), it is possible to find well isolated transitions. Recently, acetylene was used as target molecule for DBT by Hashemi et al., who probed the C_2H_2 P(25) transition of v_1+v_3 band at 1.54 µm [62] and obtained uncertainty of 85 parts over 10^6. Attempt to improve accuracy of k_B determination implementing DBT using obtained results on the $P_e(14)$ transition of the $2v_3 + v_5^1$ band of C_2H_2 molecule is discussed in this section.

The chosen transition is well isolated. The main drawback is the linestrength, which is a factor of 400 smaller than that of the $H_2^{18}O$ line used for DBT [63].

C_2H_2 spectra reported in the previous section were used for the DBT procedure. These spectra were analyzed by the same way as described in

section 4.3, but with variable Doppler width Γ_D. High quality of these spectra demonstrated in the previous section offers the possibility to retrieve the Doppler width with the high accuracy. Another two key points of any DBT experiment are (i) line fitting procedure and (ii) the choice of the line shape model. Differently from previous works, in which individual fits were performed, a global analysis approach has been applied in this work to simultaneously fit a manifold of experimental profiles across a given range of pressures, sharing a restricted number of unknown parameters, including the Doppler width. It is known that the global analysis is expected to reduce the uncertainty associated to the line shape model [69] and deviations resulting from statistical correlation among free parameters of the model [88]. The *HTP* model was applied for the line shape. The global fitting procedure was applied to the randomly selected 80 spectra corresponding 20 datasets, each of them consisted of four spectra corresponding to different pressures (10, 13, 16 and 18 Torr). The spectroscopic temperatures (as retrieved from the Doppler widths, using the CO-DATA recommended value for the Boltzmann constant [89]) are shown in Figure 4.4.1. The weighted mean of these values gives 273.13(3)K, in good agreement with the set-point, namely, 273.1602 (3) K. The resulting statistical uncertainty was 110 ppm. Then the same procedure was applied to 220 spectra corresponding to 20 datasets, each of them consisted of 11 pressures (3-30 Torr). The resulting statistical uncertainty was 40 ppm, that is better than the recent result obtained in the work [62] . As expected an increase of the number of spectra lead to a better precision. Nevertheless, an improvement of the signal-to-noise ratio (SNR) appears to be an indispensable prerequisite, in order to avoid managing thousands of spectra. In this respect, the present value of SNR of about 3500 should be

78

improved by at least a factor of 3 to reach the same level of DBT experiment based on the water vapor line [63]. To this end, the use of a non-polar molecule is advantageous. Collisions between them are less effective, while molecule adsorption and desorption from the cell walls are strongly reduced. This feature makes it possible to perform spectral averaging over a long period of time and increase the SNR without the risk of line distortion caused by a pressure variation arising from the molecular interaction with the cell.
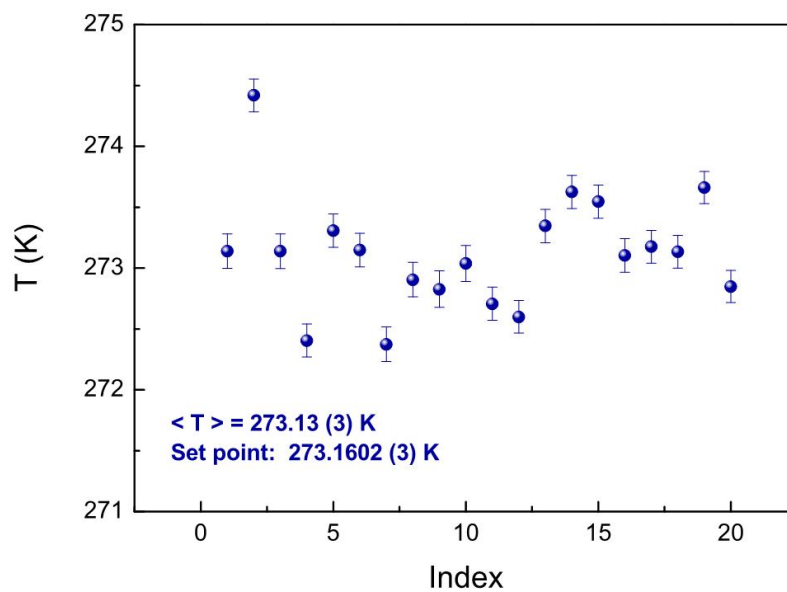

Fig. 4.4.1. Spectroscopic determinations of the gas temperature. Each point results from the global fitting of four spectra recorded at different pressures.

As for systematical deviations, the significant improvement in the spectral purity of the two lasers allowed to neglect the perturbation of the line profile associated to the so-called instrumental spectral resolution. Finally, the global fitting approach appears to be effective, reliable and robust. What is the most important thing - it does not require any preliminary knowledge about the value of collisional parameters,

circumstance that should lead to a reduction of the uncertainty associated to the line shape model.

4.5. Conclusion

The main outcome of this work is related to the level of accuracy in the retrieval of the line intensity factor of $P_e(14)$ line of $2\nu_3 + \nu_5^1$ band of C_2H_2. Detailed uncertainty budget resulted in the global uncertainty (at 1-σ) equals to 0.22%, mostly limited by two factors: (i) the uncertainty in the optical path-length determination and (ii) the statistical uncertainty. The pressure broadening and shifting parameters for the $P_e(14)$ line were measured with a precision of 0.13 and 0.18%, respectively. To the best of our knowledge, these measurements are the most accurate to date in pure C_2H_2 gas samples. The methodology can be easily extended to many other lines of different combination bands pursing the attractive idea of providing an extensive list of spectroscopic parameters. To this purpose, an optical frequency comb synthesizer could replace the reference laser, in order to have a more versatile system capable of studying lines at arbitrary frequencies.

Progress in Doppler Broadening Thermometry with the acetylene as a target molecule is reported. The $P_e(14)$ line of $2\nu_3 + \nu_5^1$ band was tested to perform DBT. The Boltzmann constant was retrieved from the shape of line with uncertainty of 40 ppm, that is the best result among k_B determined from the line shape of C_2H_2 transition. Further possible reduction of the uncertainty is discussed. It is possible by increasing number of acquired spectra and an improvement of the signal-to-noise ratio.

5. Concluding remarks

Highly-accurate spectroscopic parameters are necessary for different research fields, such as, molecular physics, metrology, environmental research, meteorology and climate physics. The methods described in the current work allowed to reach subpercent accuracy in spectroscopic line parameters determination.

The main activities of the present work can be summarized as follows:
- Development of the new approach based on OF-CEAS technique and optical frequency comb, which allows to measure CO_2 line intensities with high accuracy.
- Optimization of the dual-laser spectrometer and further increase of measurements accuracy of C_2H_2 line spectroscopic parameters. A further aim of this thesis is the optimization of Doppler-broadening thermometry as a primary method for the spectroscopic determination of the gas temperature, for the aims of the practical realization of the new Kelvin.

As for the first point, comb-calibrated laser absorption spectrometer was implemented. It is based on distributed-feedback diode laser operating at 2-μm wavelength, effectively narrowed by exploiting the optical feedback from a V-shaped high finesse optical resonator and on a comb-assisted frequency calibration unit, which is used to determine the free-spectral range of the resonator, thus providing a highly-accurate calibration of the absorption spectra. The use of the spectrometer allowed to measure line intensities of carbon dioxide with sub-percent accuracy. High accuracy of the retrieved line intensities is caused by the fact, that molecular line of interest is probed by a narrow laser (about 10 kHz), thus allowing one to

neglect the influence of the laser emission profile on the observed line shape, and that an accurate frequency scale underneath any absorption spectrum is assured. In particular, the line intensity of three isolated lines of $v_1+2v_2+v_3$ CO_2 band in the vicinity of 2 μm were investigated. Uncertainty of measurements of 0.17-0.23% was obtained, that serves the purpose of modern remote sensing missions dedicated to monitor the concentration of carbon dioxide in the Earth's atmosphere. Deviation of obtained experimental data from the most accurate to date global *ab initio* calculations is within 0.35% which can be used for the theoretical uncertainties evaluation.

Regarding the second point, dual-laser absorption spectroscopy, that is based upon a pair of phase-locked extended-cavity diode lasers, was successfully applied to investigation of the $P_e(14)$ absorption line of $2v_3+v_5$[1] band of C_2H_2 around 1.39 μm. Absolute frequency scale underneath the absorption spectra from one side, and global fitting approach with the use of the *HTP* as the line shape function, on the other side, allowed to measure line shape parameters with the unprecedented accuracy. Line intensity factor, pressure broadening and shifting parameters of the line were measured with uncertainty of 0.22%, 0.13% and 0.18%, respectively. A further outcome of this work is application of dual-laser absorption spectroscopy to Doppler Broadening Thermometry with the acetylene as a target molecule, that allowed to retrieve the Boltzmann constant from the shape of line with uncertainty of 40 ppm. This is the best result among k_B determined from the line shape of C_2H_2 transition, and is very close to the record uncertainty of 24 ppm obtained by using the DBT method. Further reduction of uncertainty is possible by increasing number of acquired spectra and an improvement of the signal-to-noise ratio.

Bibliography

[1]   L. Rothman, I. Gordon, Y. Babikov, A. Barbe, D. C. Ben-ner, P. Bernath, M. Birk, L. Bizzocchi, V. Boudon, L. Brown, A. Campargue, K. Chance, E. Cohen, L. Coudert, V. Devi, B. Drouin, A. Fayt, J.-M. Flaud, R. Gamache, J. Harri-son, J.-M. Hartmann, C. Hill, J. Hodges, D. Jacquemart, A. Jolly, J. Lamouroux, R. L. Roy, G. Li, D. Long, O. Lyulin, C. Mackie, S. Massie, S. Mikhailenko, H. Müller, O. Naumenko, A. Nikitin, J. Orphal, V. Perevalov, A. Perrin, E. Polovtseva, C. Richard, M. Smith, E. Starikova, K. Sung, S. Tashkun, J. Tennyson, G. Toon, V. Tyuterev and G. Wagner, The HITRAN2012 molecular spectroscopic database, J. Quant. Spectrosc. Radiat. Transf. 130, 4 (2013)

[2]   http://hitran.org//

[3]   N. Jacquinet-Husson, R. Armante, N. Scott, A. Chedin, L. Crepeau, C. Boutammine, A. Bouhdaoui, C. Crevoisier, V. Capelle, C. Boonne, N. Poulet-Crovisier, A. Barbe, D. C. Benner, V. Boudon, L. Brown, J. Buldyreva, A. Campargue, L. Coudert, V. Devi, M. Down, B. Drouin, A. Fayt, C. Fittschen, J.-M. Flaud, R. Gamache, J. Harrison, C. Hill, Ã. Hodnebrog, S.-M. Hu, D. Jacquemart, A. Jolly, E. JimÃl'nez, N. Lavren-tieva, A.-W. Liu, L. Lodi, O. Lyulin, S. Massie, S. Mikhailenko, H. Müller, O. Naumenko, A. Nikitin, C. Nielsen, J. Or-phal, V. Perevalov, A. Perrin, E. Polovtseva, A. Predoi-Cross, M. Rotger, A. Ruth, S. Yu, K. Sung, S. Tashkun, J. Tennyson, V. Tyuterev, J. V. Auwera, B. Voronin and A. Makie, The 2015 edition of the GEISA spectroscopic database. J. Mol. Spectrosc. 327, 31 (2016)

[4]   http://www.pole-ether.fr/etherTypo/?id=950

[5]   L. Wang, V. I. Perevalov, S. A. Tashkun, Y. Ding, and S.-M. Hu, Absolute line intensities of $^{13}C^{16}O_2$ in the 4200–8500 cm^{-1} region, J. Mol. Spectrosc. 234, 84, (2005)

[6]   B. V. Perevalov, A. Campargue, B. Gao, S. Kassi, S. A. Tashkun, and V. I. Perevalov, New CW-CRDS measurements and global modeling of $^{12}C^{16}O_2$ absolute line intensities in the 1.6 μm region J. Mol. Spectrosc. 252 , 190 (2008);

[7]   K. F. Song , S. Kassi, S. A. Tashkun, V. I. Perevalov, and A. Campargue,   High   sensitivity *CW*-cavity   ring   down   spectroscopy of $^{12}CO_2$ near 1.35 μm (II): New observations and line intensities modeling, J. Quant. Spectrosc. Radiat. Transf. 111, 332 (2010)

[8]   D. Boudjaadar, J.-Y. Mandin, V. Dana, N. Picqué, and G. Guelachvili, $^{12}C^{16}O_2$ line intensity measurements around 1.6 μm, J. Mol. Spectrosc. 236 , 158 (2006)

[9]   B. Bézard, A. Fedorova, J.L. Bertaux, A. Rodin, O. Korablev, The 1.10- and 1.18-μm nightside windows of Venus observed by SPICAV-IR aboard Venus Express, Icarus 216, 173 (2011)

[10] GOSAT   M. Yokomizo, Greenhouse gases Observing SATellite (GOSAT) ground systems. Fujitsu Sci. Tech. J. 44:410 (2008) http://www.gosat.nies.go.jp/en/

[11] D.R. Thompson, D.C. Benner, L.R. Brown, D. Crisp, V.M. Devi, Y.B. Jiang, et al. Atmospheric validation of high accuracy CO_2 absorption coefficients for the OCO-2 mission, J. Quant. Spectrosc. Radiat. Transf. 113, 2265 (2012)

[12] http://oco.jpl.nasa.gov

[13]   http://www.gosat.nies.go.jp/en/

[14]   http://www.iup.uni-bremen.de/carbonsat/

[15]   D. Jacquemart, F. Gueye, O.M. Lyulin, E.V. Karlovets, D. Baron, V.I. Perevalov, Infrared spectroscopy of CO_2 isotopologues from 2200 to 7000 cm^{-1}: characterizing experimental uncertainties of positions and intensities, J. Quant. Spectrosc. Radiat. Transf. 113, 961 (2012)

[16]   O.L. Polyansky, K. Bielska, M. Ghysels, L. Lodi, N. F. Zobov, J. T. Hodges, and J. Tennyson, High-Accuracy CO_2 Line Intensities Determined from Theory and Experiment, Phys. Rev. Lett. 114, 243001 (2015)

[17]   E. Zak, J. Tennyson, O. L. Polyansky, L. Lodi, N. F. Zobov, S. A. Tashkun and V. I. Perevalov, Room temperature linelists for CO_2 asymmetric isotopologues with *ab initio* computed intensities, J. Quant .Spectrosc. Radiat. Transf. 177, 31 (2016)

[18]   R. Whitby and E. Altwicker, Acetylene in the atmosphere: sources, representative ambient concentrations and ratios to other hydrocarbons, Atmospheric Environment 12, 1289 (1978)

[19]   R. Zander, C. Rinsland, D. Ehhalt, J. Rudolph, and P. Demoulin, Vertical column abundances and seasonal cycle of acetylene, C_2H_2, above the Jungfraujoch station, derived from IR Solar observations. J. Atmos. Chem. 13 , 359 (1991)

[20] D. Horn, J. M. McAfee, A. M. Winer, K. C. Herr, and G. C. Pimentel, The composition of the Martian atmosphere: Minor constituents, Icarus 16 , 543 (1972)

[21] P. V. Sada, G. L. Bjoraker, D. E. Jennings, G. H. McCabe, and P. N. Romani, Observations of CH_4, C_2H_6, and C_2H_2 in the Stratosphere of Jupiter, Icarus 136, 192 (1998)

[22] R. J. Vervack, B. R. Sandel, and D. F. Strobel, New perspectives on Titan's upper atmosphere from a reanalysis of the Voyager 1 UVS solar occultations, Icarus 170, 91 (2004)

[23] M. Burgdorf, G. Orton, J. van Cleve, V. Meadows, and J. Houck, Detection of new hydrocarbons in Uranus' atmosphere by infrared spectroscopy, Icarus 184, 634 (2006)

[24] J. Bishop, S. Atreya, F. Herbert, and P. Romani, Reanalysis of voyager 2 UVS occultations at Uranus: Hydrocarbon mixing ratios in the equatorial stratosphere, Icarus 88, 448 (1990)

[25] B. Conrath, F. M. Flasar, R. Hanel, V. Kunde, W. Maguire, J. Pearl, J. Pirraglia, R. Samuelson, P. Gierasch, A. Weir, B. Bezard, D. Gautier, D. Cruikshank, L. Horn, R. Springer, and W. Shaffer, Infrared Observations of the Neptunian System, Science 246, 1454 (1989)

[26] J. Crovisier, Infrared observations of volatile molecules in comet Hale-Bopp. Earth Moon Planets 79, 125 (1999)

[27] E.L. Gibb, K.A. Van Brunt, S.D. Brittain, T.W. Rettig, Warm HCN, C_2H_2, and CO in the disk of GV TAU Astrophys. J. 660 1572 (2007)

[28] J.H. Lacy, N.J. Evans II, J.M. Achtermann, D.E. Bruce, J.F. Arens, J.S. Carr, Discovery of interstellar acetylene, Astrophys. J. 342, L43, (1989)

[29]   J.T. Van Loon, J.R. Marshall, M. Cohen, M. Matsuura, P.R. Wood, I. Yamamura, A.A. Zijlstra, Very Large Telescope three micron spectra of dust-enshrouded red giants in the Large Magellanic Cloud, Astron. Astrophys. 447, 971 (2006)

[30]   V. Duflot, C. Wespes, L. Clarisse, D. Hurtmans, Y. Ngadi, N. Jones, C. Paton-Walsh, J. Hadji-Lazaro, C. Vigouroux, M. De Mazi`ere, J.-M. Metzger, E. Mahieu, C. Servais, F. Hase, M. Schneider, C. Clerbaux, and P.-F. Coheur, Acetylene (C_2H_2) and hydrogen cyanide (HCN) from IASI satellite observations: global distributions, validation, and comparison with model, Atmos. Chem. Phys. 15, 10509 (2015)

[31]   L. Gianfrani, Linking the thermodynamic temperature to an optical frequency: recent advances in Doppler broadening thermometry, Phil. Trans. R. Soc. London A 374, 20150047(2016)

[32]   A.Castrillo, E. Fasci, G.Galzerano, G. Casa, P. Laporta, and L. Gianfrani. Offset-frequency locking of extended-cavity diode lasers for precision spectroscopy of water at 1.38mm. Opt. Express. 18(21), 21851 (2010)

[33]   R.H. Dicke, The effect of collisions upon the Doppler width of spectral line, Phys. Rev. 89, 472 (1953)

[34]   L. Galatry, Simultaneous effect of Doppler and foreign gas broadening on spectral lines. Phys. Rev. 122, 1218 (1960)

[35]   S.G. Rautian, I.I. Sobel'man, Influence of collisions on Doppler broadening of spectral lines, Usp. Fiz. Nauk. 90, 209 (1966)

[36]   S. Chandrasechar, Stochastic problems in physics and astronomy, Rev. Mod. Phys. 15,1 (1943)

[37]   M. Hartmann, C. Boulet, D. Robert, Collisional effects on molecular spectra: laboratory experiments and models, consequences for applications, Amsterdam: Elsevier Science (2008)

[38]   F. Rohart, L. Nguyen, J. Buldyreva, J.M. Colmont, G. Wlodarczak, Line-shapes of the 172 and 602 GHz rotational transitions of HC15N, J. Mol .Spectrosc. 246, 213 (2007)

[39]   J. Berman, Speed-dependent collisional width and shift parameters in spectral profiles, J. Quant. Spectrosc. Radiat. Transf. 12,1331 (1972)

[40]   F. Rohart, H. Mäder, H.W. Nicolaisen, Speed dependence of rotational relaxation induced by foreign gas collisions: studies on CH_3F by millimeter wave coherent transients, J. Chem. Phys. 101, 6475 (1994)

[41]   N.H. Ngo, D. Lisak, H. Tran, J.-M. Hartmann, An isolated line-shape model to go beyond the Voigt profile in spectroscopic databases and radiative transfer codes, J. Quant. Spectrosc. Radiat. Transf. 129, 89 (2013)

[42]   A. S. Pine, R. Ciuryło, Multispectrum Fits of Ar-Broadened HF with a Generalized Asymmetric Lineshape: Effects of Correlation, Hardness, Speed Dependence, and Collision Duration, J. Mol. Spectrosc. 208 , 180 (2001)

[43]   J. Tennyson, P. F. Bernath, A. Campargue, A. G. Császár, L. Daumont, R. R. Gamache, J. T. Hodges, D. Lisak, O. V. Naumenko, L. S. Rothman, H. Tran, N. F. Zobov, J. Buldyreva,C. D. Boone, M. D. D. Vizia, L. Gianfrani, J.-M. Hartmann, R. McPheat, D. Weidmann, J. urray, N. H. Ngo and O. L.Polyansky, Recommended isolated-line profile for representing high-resolution spectroscopic transitions (IUPAC Technical Report), Pure and Applied Chemistry 86, 1931 (2014)

[44]   H. Kogelnik, T. Li, Laser Beams and Resonators, Applied Optics 5, 10, 1550 (1966)

[45]   J. L. Hall, "Nobel Lecture: Defining and measuring optical frequencies" , Rev. Mod. Phys.78(4), 1279 (2006)

[46]   T. W. Haensch, "Nobel Lecture: Passion for precision", Rev. Mod. Phys. 78(4), 1297 (2006);

[47]   D. J. Jones et al., "Carrier-Envelope Phase Control of Femtosecond Mode-Locked Lasers and Direct Optical Fre-quency Synthesis," Science. 288(5466), 635 (2000)

[48]   F. Tauser, A. Leitenstorfer, and W. Zinth, "Amplified fem-tosecond pulses from an Er:fiber system: Nonlinear pulse shortening and self-referencing detection of the carrier-envelope phase evolution," Opt. Express 11(6), 594–600 (2003)

[49]   K. R. Preston, K. C. Woollard, and K. H. Cameron, External cavity controlled single longitudinal mode laser transmitter module, Electron. Lett. 17(24), 931 (1981)

[50]   R. Wyatt and W. J. Devlin, 10 kHz linewidth 1.5 µm InGaAsP external cavity laser with 55 nm tuning range, Electron. Lett. 19, 110(1983)

[51]   S. Kobayashi and T. Kimura, Injection locking in AlGaAs semiconductor laser, IEEE J. Quant. Electron. 17(5), 681 (1981)

[52]   E. Fasci, T. A. Odintsova, A. Castrillo, M. D. De Vizia, A. Merlone, F. Bertiglia, L. Moretti, and L. Gianfrani, Dual-laser absorption spectroscopy of C2H2 at 1.4 µm, Phys. Rev. A 93, 042513 (2016)

[53]   R. Lang, K. Kobayashi. External Optical Feedback Effects on Semiconductor Injection Laser Properties. External Optical Feedback Effects on Semiconductor Injection Laser Properties, IEEE Journal of Quantum Electronics, 16, 3, 347 (1980)

[54]   B. Dahmani, L. Hollberg, R. Drullinger, Frequency stabilization of semiconductor lasers by resonant optical feedback. Opt. Lett. 12, 876 (1987)

[55]   J. Morville, S. Kassi, M. Chenevier, D. Romanini, Fast, low-noise, mode-by-mode, cavity-enhanced absorption spectroscopy by diode-laser self-locking, Appl. Phys. B 80, 1027 (2005)

[56]   R. Wehr, S. Kassi, D. Romanini, L. Gianfrani, Optical feedback cavity-enhanced absorption spectroscopy for in situ measurements of the ratio $^{13}C^{12}C$ in CO_2, Appl. Phys. B 92, 459 (2008)

[57]   H. Dinesan, E. Fasci, A. Castrillo, and L. Gianfrani, Absolute frequency stabilization of an extended-cavity diode laser by means of noise-immune cavity-e nhanced optical heterodyne molecular spectroscopy, Opt. Lett. 39(7), 2198 (2014)

[58]   H. Dinesan, E. Fasci, A. D'Addio, A. Castrillo, and L. Gianfrani, Characterization of the frequency stability of an optical frequency standard at 1.39 μm based upon noise-immune cavity-enhanced optical heterodyne molecular spectroscopy, Opt. Express 23, 1757 (2015)

[59]   M. de Podesta, R. Underwood, G. Sutton, P. Morantz, P. Harris, D.F. Mark, F.M. Stuart, G. Vargha, G. Machin. A low-uncertainty measurement of the Boltzmann constant. Metrologia 50, 354 (2013)

[60]   C. Gaiser, T. Zandt, B. Fellmuth, J. Fischer, O. Jusko, W. Sabuga, Improved determination of the Boltzmann constant by dielectric-constant gas thermometry, Metrologia 50, L7 (2013)

[61]   G. Casa, A. Castrillo, G. Galzerano, R. Wehr, A. Merlone, D. Di Serafino, P. Laporta, L. Gianfrani, Primary gas thermometry by means of laser-absorption spectroscopy: determination of the Boltzmann constant, Phys. Rev. Lett. 100, 200801 (2008)

[62]   R. Hashemi, C. Povey, M. Derksen, H. Naseri, J. Garber and A. Predoi-Cross, Doppler broadening thermometry of acetylene and accurate measurement of the Boltzmann constant, J. Chem. Phys. 141, 214201(2014)

[63]   L. Moretti, A. Castrillo, E. Fasci, M. D. De Vizia, G. Casa, G. Galzerano, A. Merlone, P. Laporta and L. Gianfrani, Determination of the Boltzmann constant by means of precision measurements of $H_2^{18}O$ line shapes at 1.39 μm, Phys. Rev. Lett. 111, 060803 (2013)

[64]   G. Casa, A. Castrillo, G. Galzerano, R. Wehr, A. Merlone, D. Di Serafino, P. Laporta, L. Gianfrani, Primary gas thermometry by means of laser-absorption spectroscopy: determination of the Boltzmann constant, Phys. Rev. Lett. 100, 200801 (2008)

[65]   G. Casa, D. A. Parretta, A. Castrillo, R. Wehr and L. Gianfrani, Highly accurate determinations of CO_2 line strengths using intensity-stabilized diode laser absorption spectrometry, J. Chem. Phys. 127, 084311 (2007)

[66]   G. Casa, R. Wehr, A. Castrillo, E. Fasci and L. Gianfrani, The line shape problem in the near-infrared spectrum of self-colliding CO_2

molecules: Experimental investigation and test of semiclassical models. J. Chem. Phys. 130, 184306 (2009)

[67] G. Wuebbeler, G. J. P. Viquez, K. Jousten, O. Werhahn, C. Elster, Comparison and assessment of procedures for calculating the R(12) line strength of the $v_1+2v_2+v_3$ band of CO2, J. Chem. Phys. 135, 204304 (2011)

[68] A. Castrillo, G. Gagliardi, G. Casa, and L. Gianfrani, Combined interferometric and absorption-spectroscopic technique for determining molecular line strengths: Applications to CO_2, Phys. Rev. A 67, 062503 (2003)

[69] P. Amodio, M. D. De Vizia, L. Moretti and L. Gianfrani, Investigating the ultimate accuracy of Doppler-broadening thermometry by means of a global fitting procedure, Phys. Rev. A 92, 032506 (2015)

[70] Malengo and F. Pennecchi, A weighted total least-squares algorithm for any fitting model with correlated variables, Metrologia 50, 6, 654 (2013)

[71] Gordon and et al, J. Quant. Spectrosc. Radiat. Transf.,1

[72] H. W. Yoon, J. J. Butler, T. C. Larason and G. P. Eppeldauer, Linearity of InGaAs photodiodes, Metrologia 40, S154 (2003)

[73] G. Larcher, X. Landsheere, M. Schwell and H. Tran, Spectral shape parameters of pure CO_2 transitions near 1.6 μm by tunable diode laser spectroscopy, J. Quant. Spectrosc. Radiat. Transf. 164, 82 (2015)

[74] A .F. Seleznev, G.V. Fedoseev, M. A. Koshelev, M.Yu. Tretyakov, Shape of collision-broadened lines of carbon monoxide, J. Quant. Spectrosc. Radiat. Transf. 161, 171 (2015)

[75]   D. Jacquemart, N. Lacome, J.-Y. Mandin, V. Dana, H. Tran, F.Gueye, O. Lyulin, V. Perevalov, and L. R´egalia-Jarlot, The IR spectrum of $^{12}C_2H_2$: Line intensity measurements in the 1.4 μm region and update of the databases. J. Quant. Spectrosc. Radiat. Transf. 110, 717 (2009)

[76]   O. Lyulin, J. V. Auwera, and A. Campargue, The Fourier transform absorption spectrum of acetylene between 7000 and 7500 cm^{-1}. J. Quant. Spectrosc. Radiat. Transf. 160, 85 (2015)

[77]   S. Arteaga, C. Bejger, J. Gerecke, J. Hardwick, Z. Martin, J. Mayo, E. McIlhattan, J.-M. Moreau, M. Pilkenton, M. Polston, B. Robertson, and E. Wolf, Line broadening and shift coefficients of acetylene at 1550 nm, J. Mol. Spectrosc. 243, 253 (2007)

[78]   S. Robert, B. Amyay, A. Fayt, G. D. Lonardo, L. Fusina, F. Tamassia, and M. Herman, Vibration−Rotation Energy Pattern in Acetylene: $^{13}CH^{12}CH$ up to 10120 cm^{-1} , J Phys. Chem. A 113(47), 13251 (2009)

[79]   S. Robert, M. Herman, A. Fayt, A. Campargue, S. Kassi, A. Liu, L. Wang, G. D. Lonardo, and L. Fusina, Acetylene, $^{12}C_2H_2$: new CRDS data and global vibration-rotation analysis up to 8600 cm^{-1}, Mol. Phys.106, 2581 (2008)

[80]   S. Twagirayezu, M. J. Cich, T. J. Sears, C. P. McRaven, and G. E. Hall, Frequency-comb referenced spectroscopy of v_4- and v_5-excited hot bands in the 1.5 μm spectrum of C_2H_2, J. Mol. Spectrosc. 316, 64 (2015)

[81]   C. P. McRaven, M. Cich, G. Lopez, T. J. Sears, D. Hurtmans, and A. Mantz, Frequency comb-referenced measurements of self- and nitrogen-

broadening in the $v_1 + v_3$ band of acetylene, J. Mol. Spectrosc. 266, 43 (2011)

[82] D. Forthomme, M. Cich, S. Twagirayezu, G. Hall, and T. Sears, Application of the Hartmann–Tran profile to precise experimental data sets of $^{12}C_2H_2$, J. Quant. Spectrosc. Radiat. Transf. 165, 28 (2015)

[83] J. Ye, L.-S. Ma, and J. L. Hall, Sub-Doppler optical frequency reference at 1.064 μm by means of ultrasensitive cavity-enhanced frequency modulation spectroscopy of a C_2HD overtone transition, Opt. Lett. 21, 1000 (1996)

[84] A. Merlone, F. Moro, A. Castrillo, and L. Gianfrani, Design and Capabilities of the Temperature Control System for the Italian Experiment Based on Precision Laser Spectroscopy for a New Determination of the Boltzmann Constant, Int. J. Thermophys. 31, 1360 (2010)

[85] D. Jacquemart, J.-Y. Mandin, V. Dana, L. R´egalia-Jarlot, J.-J. Plateaux, D. D´ecatoire, and L. Rothman, The spectrum of acetylene in the 5-μm region from new line-parameter measurements, J. Quant. Spectrosc. Radiat. Transf. 76 , 237 (2003)

[86] Malengo and F. Pennecchi, A weighted total least-squares algorithm for any fitting model with correlated variables, Metrologia 50(6), 654 (2013)

[87] R. Gamache, S. Kennedy, R. Hawkins, and L. Rothman, Total internal partition sums for molecules in the terrestrial atmosphere. J. Mol. Struct. 517-518, 407 (2000)

[88]   P. Amodio, L. Moretti, A. Castrillo and L. Gianfrani, Line-narrowing effects in the near-infrared spectrum of water and precision determination of spectroscopic parameters, J. Chem. Phys. 140 , 044310 (2014)

[89]   P. J. Mohr, B. N. Taylor and D. B. Newell, CODATA recommended values of the fundamental physical constants: 2010, Rev. Mod. Phys. 84, 1527 (2012)

List of publications

Papers

[1]   M. D. De Vizia, T. Odintsova, and L. Gianfrani, Hyperfine structure effects in Doppler-broadening thermometry on water vapor at 1.4 μm, Metrologia 53, 800 (2016)

[2]   E. Fasci, T. A. Odintsova, A. Castrillo, M. D. De Vizia, A. Merlone, F. Bertiglia, L. Moretti, and L. Gianfrani, Dual-laser absorption spectroscopy of C2H2 at 1.4 μm, Phys. Rev. A 93, 042513 (2016)

[3]   A. Castrillo, M.D. De Vizia, E. Fasci, T. Odintsova, L. Moretti and L. Gianfrani. Doppler-Broadening Gas Thermometry at 1.39 μm: Towards a New Spectroscopic Determination of the Boltzmann Constant. World scientific, Laser Spectroscopy, Proceedings of the XXII International Conference on Laser Spectroscopy (ICOLS2015), Singapore, 28 June – 3 July 2015, p. 31-41

[4]   T. A. Odintsova, E. Fasci, L. Moretti, E.J. Zak, O.L.Polyansky, J. Tennyson, L.Gianfrani, A. Castrillo, Highly-accurate intensity factors of pure CO_2 lines near 2 μm, Journal of Chemical Physics 146, 244309 (2017)

Abstracts

[1]   E. Fasci, A. Castrillo, T. Odintsova, M. D. De Vizia, L. Moretti, and L. Gianfrani. Dual-laser absorption spectroscopy of C2H2 at 1.4 μm. HRMS, 24th Colloquium, Dijon, France, 24 - 28 Aug, 2015, Abstract of Reports: p319, N18

[2]   E. Fasci, M.D. De Vizia, H. Dinesan, T. Odintsova, A. Castrillo, L. Moretti, A. Merlone, and L. Gianfrani. Primary gas thermometry based upon dual-laser absorption spectroscopy. Abstract of Reports: FOTONICA 2015, Turin, Italy, 6-8 May, 2015

[3]   E. Fasci, M.D. De Vizia, H. Dinesan, T. Odintsova, A. Castrillo, L. Moretti, A. Merlone, and L. Gianfrani. Doppler-broadened dual-laser absorption spectroscopy for thermodynamic temperature measurements. Abstract of Reports: Italian National Conference on Condensed Matter Physics FisMat2015, Palermo, Italy, 28 Sept. - 2 Oct., 2015

[4]   T. Odintsova, A. Castrillo, M.D. De Vizia, E. Fasci and L. Gianfrani. Comb-calibrated line intensity measurements for CO_2 spectra at 2 μm. Abstract of Reports: FLAIR 2016, 12-16 Sept., 2016